Control Theory Tech, Vol. 16, No. 4, pp. 261–283, November 2018

Control Theory and Technology

http://link.springer.com/journal/11768

Embedded model control: Reconciling modern control theory and error-based control design

Enrico CANUTO†, Carlo NOVARA, Luigi COLANGELO

Politecnico di Torino, Italy

Received 27 June 2018; revised 23 July 2018; accepted 23 July 2018

Abstract

The paper addresses the problem of reconciling the modern control paradigm developed by R. Kalman in the sixties of the past century, and the centenary error-based design of the proportional, integrative and derivative (PID) controllers. This is done with the help of the error loop whose stability is proved to be necessary and sufficient for the close-loop plant stability. The error loop is built by cascading the uncertain plant-to-model discrepancies (causal, parametric, initial state, neglected dynamics), which are driven by the design model output and by arbitrary bounded signals, with the control unit transfer functions. The embedded model control takes advantage of the error loop and its equations to design appropriate algorithms of the modern control theory (state predictor, control law, reference generator), which guarantee the error loop stability and performance. A simulated multivariate case study shows modeling and control design steps and the coherence of the predicted and simulated performance.

Keywords: Modern control theory, error-based design, embedded model control, error loop, disturbance rejection

DOI https://doi.org/10.1007/s11768-018-8130-1

1 Introduction

In the 80's of the past century, J. Han of the Chinese Academy of Sciences, Beijing, China, in a suite of Chinese-written papers (see [1] for a more recent English summary) pointed out the difficulties of the *modern control paradigm* proposed by R. Kalman in his seminal paper "On the general theory of control systems" [2] in front of the real plant uncertainty. Z. Gao observed in [3] that the robust control design is a *paradox* that looks unsolvable within the modern control paradigm. The stunning fact is that, after sixty years of modern control theory and myriads of publications, the proportional, integrative and derivative (PID) controller, formulated around 1920 and applied to ship steering by [4, 5], is still the work-horse of automatic control in all the fields of application. The argument of J. Han and Z. Gao [1, 3, 6] is that PID design and tuning (the *error-based design paradigm*) is substantially model independent and only guaranteed by the experimental per-

†Corresponding author.
E-mail: enrico.canuto@polito.it.

formance of the measured tracking error between reference and plant measurements. It seems evident that a fracture exists between a well-established and mature mathematical theory and a centenary successful engineering practice.

Is a reconciliation workable and by which means? The goal of this paper is to prove that reconciliation is feasible and that robust control theories and design methodologies exist and have been in-field applied. The main design objective is to guarantee stability and performance of a real control system in the presence of a given class of uncertain discrepancies between real plant and mathematical model.

The key result of the paper in Section 2.3.3 is that, given a suitable mathematical model of the plant and the required performance, Kalman theory allows a class of parameterized controllers to be designed and tuned in order to guarantee stability and performance in presence of a well-defined class of uncertain discrepancies. The tool for controller tuning and performance verification is the *error loop* [7], in which plant and model discrepancies are appropriately filtered by the controller itself for guaranteeing stability and requirements. A theorem proves that the error loop stability is a necessary and sufficient condition for the stability of the closed-loop plant.

The paper is organized into three steps.

Section 2 starts by briefly recalling Kalman theory and objectives [2] and the unstructured uncertainty defined by the robust stability theory of J. C. Doyle and G. Stein [8]. Both theories together with the small-gain theorem of G. Zames [9] are the foundations of the theory of F. Donati and M. Vallauri [10]. The theory exploits the machinery of the input-output norm of dynamic operators to define concept and method of "almost-linear plants". In essence, the output error norm between almost-linear plant and model can be made smaller than the model output norm: in other terms, the fractional error can be brought to be less than 100%. Though insufficient to invoke the small-gain theorem for the whole loop including plant and controller, it facilitates the model-based design of a feedback controller that guarantees a loop gain less than unit and therefore closed-loop stability. The stabilizable loop, referred to as the error loop in [7], is proved to be the cascade of the unstructured uncertainty and of two model-based closed loop transfer functions.

Section 3 traces the path from Section 2 to the embedded model control (EMC) [7,11]. First it goes beyond the unstructured uncertainty by separating four uncertainty classes: initial state, parametric and causal uncertainty and neglected dynamics, and proves that whereas parametric and causal uncertainty must be canceled on the plant, neglected dynamics contribution must be blocked from entering the controller itself. The controller architecture is similar to that of F. Donati and M. Vallauri [10] as well as to the internal model control [12] and the active disturbance rejection control [3]. As a second point, design and embedded model are distinguished. The design model, which surrogates the plant, includes the whole uncertainty class. The uncertainty simplifies to the causal uncertainty in the embedded model, which is the core of the controller and is the basis for the controller design. Design model and controller allow to build design equations which relate tracking and other errors to the uncertainty class elements (the error loop equations) and guide the robust controller tuning (pole placement) through analytic inequalities relating requirements, controller parameters (closed-loop poles) and uncertainty bounds.

Models, equations and pole placement of Section 3 are employed in Section 4 to solve a well-known multivariate and nonlinear control problem [13], which does not admit the normal form of the feedback linearization [14] and is non-minimum phase in the linear approximation. Analytic design versus uncertainty is checked by simulated trials.

2 The robust design problem

2.1 R. Kalman's theory

In his seminal paper on the "General theory of control systems" [2], R. Kalman's ultimate objective was to answer two questions:

1) What kind and how much information are needed to achieve a desired type of control?

2) What intrinsic properties characterize a given unalterable plant as far as control is concerned?

The aim is that of "initiating study of the pure theory of control, imitating the spirit of Shannon's investigations in the theory of information", but "avoiding the well-known difficulty of Shannon's theory: methods of proof which are impractical for actually constructing practical solutions". To this end, "only constructive methods are employed" but restricted to "dynamic systems with a finite dimensional state space and linear transition functions, excited by an uncorrelated stationary Gaussian

random process". R. Kalman did not explicitly answered the above questions but proved that "the general problem of *optimal regulation* is solvable if and only if the plant is *completely controllable*", and that "*the optimal state prediction* which solves the Wiener filtering problem" requires the *complete observability* of a linear dynamic system excited by a Gaussian random process. The concepts of *plant* ("physical object") and *mathematical model* ("dynamic system") are distinguished; but the paper concentrates on the model properties with the explicit assumption (page 482, [2]) that model input and output are at the same time plant input and output. The *inherent uncertainty* of the input and output random processes is just seen as a model (and plant) property.

Sufficient conditions for linear time-invariant (*LTI*) *model stabilizability*. In summary, although not explicitly stated and by confounding plant with model, *controllability and observability* (briefly *minimality*) are proved to be *sufficient* conditions for designing asymptotically stable (AS) LTI regulators and predictors, and *necessary and sufficient* for their optimality, independently of the uncorrelated stationary Gaussian random processes (with bounded covariance in the discrete-time (DT) case and bounded spectral density (SD) in the continuous-time (CT) case) which are applied to the model. Minimality is only sufficient for the stabilizability since also non-minimal LTI models may be feedback stabilized.

2.2 Doyle-Stein's robust stability

A first step toward a theory of *uncertain dynamic systems* and their stabilizability was done in 1981 by J. C. Doyle and G. Stein [8]. The input-output LTI design model expressed by the minimal transfer matrix $M(s = \mathrm{j}2\pi f), f \geqslant 0$ (without pole-zero cancellation), is complemented by an unknown but bounded perturbation $\Delta P(\mathrm{j}f)$, whose bound is defined by the set membership statement:

$$\begin{aligned} 0 &< \sigma^2_{\max}(\Delta P(\mathrm{j}f)) \\ &= \lambda_{\max}(\Delta P^{\mathrm{T}}(-\mathrm{j}f)\Delta P(\mathrm{j}f)) \leqslant \delta(\mathrm{j}f), \end{aligned} \tag{1}$$

where $f \geqslant 0$ and $\sigma_{\max}$ is the largest singular value of $\Delta P(\mathrm{j}f)$. The uncertainty defined in (1) which does not postulate any specific expression of $\Delta P(\mathrm{j}f)$ is referred to as *unstructured uncertainty*. Since matrix algebra admits multiplication (though not commutative), the authors of [8] recognized that uncertainty can be expressed in a multiplicative way as

$$P(\mathrm{j}f) = M(\mathrm{j}f) + \Delta P(\mathrm{j}f) = (I + \partial P(\mathrm{j}f))M(\mathrm{j}f), \tag{2}$$

where, if M is invertible, the form

$$\partial P(\mathrm{j}f) = P(\mathrm{j}f)M^{-1}(\mathrm{j}f) - I \tag{3}$$

takes the meaning of a *fractional/relative error*. Comparison of the set membership uncertainty in (1) with the uncertainty of a stationary Gaussian random process postulated by the R. Kalman theory in [2], though of interest, is left to the reader.

Sufficient conditions for robust LTI stabilizability. Given a feedback $F(\mathrm{j}f)$ that stabilizes the closed-loop complementary sensitivity (CS) $V(\mathrm{j}f)$ defined by $V = (I + FM)^{-1}FM$, and the additional assumption of equal number of unstable poles in FP and FM, the "robust" closed-loop sufficient stability condition amounts to the small-gain inequality:

$$\sigma_{\max}(\partial P(\mathrm{j}f))\sigma_{\max}(V(\mathrm{j}f)) < 1, \quad f \geqslant 0. \tag{4}$$

2.3 Donati-Vallauri's robust control theory and the Han's paradox

2.3.1 The input-output unstructured uncertainty

A further step was made in 1984 by F. Donati and M. Vallauri [10] by defining the unstructured uncertainty in terms of the input-output norm of dynamic operators (not necessarily linear) and by employing the same machinery of the *small-gain theorem* [11] of G. Zames [9]. In this framework, given, for instance, the finite norm of a time-truncated vector signal:

$$\|v\|_{2,H} = \sqrt{\int_0^H |v(\tau)|^2 \,\mathrm{d}\tau} < \infty, \quad H < \infty, \tag{5}$$

where $|v(\tau)|$ is the vector Euclidean norm, a dynamic system $\boldsymbol{y} = P(\boldsymbol{u})$ is said to be *finite-gain stable* if there exists a pair $\{\eta, \delta\}$ of finite reals such that

$$\|\boldsymbol{y}\|_{2,H} \leqslant \eta\|\boldsymbol{u}\|_{2,H} + \delta, \quad 0 \leqslant H < \infty, \tag{6}$$

where, in the sequel, $\|\cdot\| = \|\cdot\|_{2,H}$ unless otherwise said. Time truncation corresponds to the frequency resolution $\Delta f \geqslant H^{-1}$. i) Given a real plant (distinguished from mathematical models) defined by an unknown input-output operator $\boldsymbol{y} = P(\boldsymbol{u})$ and an admissible input set $\boldsymbol{\mathcal{U}}$; ii) given a minimal linear dynamic model $\boldsymbol{y}_{\mathrm{m}} = M\boldsymbol{u}$ (respecting causality) and the model error $\tilde{\boldsymbol{y}}_{\mathrm{m}} = \boldsymbol{y} - \boldsymbol{y}_{\mathrm{m}}$,

plant and model admit an *unstructured uncertainty*, if and only if a finite pair $\{\eta_P, \delta_P\}$ exists such that

$$\begin{aligned}\|\tilde{\boldsymbol{y}}_{\mathrm{m}}\| =&\|\boldsymbol{y}-\boldsymbol{y}_{\mathrm{m}}\| \leqslant \eta_P\|\boldsymbol{u}\|+\delta_P,\\ &0 \leqslant \eta_P,\ \delta_P < \infty,\ \boldsymbol{u}\in\mathcal{U}.\end{aligned} \tag{7}$$

In [9] and [10], the input-output operators map time signals defined in a Banach space [15]. Here, we restrict to a Hilbert space [15] defined by the scalar product $<\boldsymbol{v},\boldsymbol{w}>$ of the complex vectorial functions $\boldsymbol{v}$ and $\boldsymbol{w}$ for any finite $0 \leqslant H < \infty$:

$$\begin{cases}\langle \boldsymbol{v},\boldsymbol{w}\rangle = \int_0^H \boldsymbol{v}^*(\tau)\boldsymbol{w}(\tau)\mathrm{d}\tau < \infty,\ \ H<\infty,\\ \|\boldsymbol{v}\|^2 = \langle \boldsymbol{v},\boldsymbol{v}\rangle,\end{cases} \tag{8}$$

where $\boldsymbol{v}^*$ is the transpose conjugate of $\boldsymbol{v}$. In the LTI case and in the Hilbert space, the input-output norm of a dynamic operator M is defined in the frequency domain by

$$\|M\|_\infty = \sup_{\|\boldsymbol{u}\|\leqslant 1}\frac{\|M\boldsymbol{u}\|}{\|\boldsymbol{u}\|} = \sup_f \sigma_{\max}(M(\mathrm{j}f)). \tag{9}$$

The operator norm $\|\cdot\|_\infty$ is known as the H_∞ norm and $\sigma_{\max}$ denotes the largest singular value. In the following, the supremum sup will be changed into maximum max by slightly shifting the imaginary axis poles into the left half-plane.

As in (3), we prefer converting (8) into a fractional uncertainty, by replacing $\|\boldsymbol{u}\|$ with $\|\boldsymbol{y}_{\mathrm{m}}\|$. This requires the replacement of $\boldsymbol{u}$ with $\boldsymbol{y}_{\mathrm{m}}$ in $P(\cdot)$ and the approximate inversion of M by means of a suitable feedback F_u as in Fig. 1.

As a result, the input set $\mathcal{U}$ becomes restricted to the subset

$$\mathcal{U}^* : \{\boldsymbol{u} = V_u M^{-1}\boldsymbol{y}_{\mathrm{m}} = V_u\boldsymbol{u},\ \boldsymbol{u}\in\mathcal{U}\}, \tag{10}$$

where $V_u = (I+F_uM)^{-1}F_uM$ is AS and, being a complementary sensitivity, plays the role of a low-pass (LP) filter capable of attenuating the high-frequency (HF) components of $\boldsymbol{u}$. This is the dual effect of the time truncation in (5), since the frequency bandwidth (BW) f_u of V_u constrains the time resolution Δt of $\boldsymbol{u}$ to satisfy $\Delta t \geqslant 1/(2f_u)$. If M is a DT model with time unit T, the inverse approximation is accurate as soon as $\Delta t < T$. It is now possible to define the *fractional error operator* $\partial P(\boldsymbol{y}_{\mathrm{m}})$:

$$\tilde{\boldsymbol{y}}_{\mathrm{m}} = \boldsymbol{y}-\boldsymbol{y}^*_{\mathrm{m}} = P(V_uM^{-1}\boldsymbol{y}_{\mathrm{m}}) - V_u\boldsymbol{y}_{\mathrm{m}} = \partial P(\boldsymbol{y}_{\mathrm{m}}), \tag{11}$$

and to redefine the *unstructured uncertainty* by means of the following input-output norm inequality:

$$\begin{aligned}\|\tilde{\boldsymbol{y}}_{\mathrm{m}}\| =&\|\boldsymbol{y}-\boldsymbol{y}^*_{\mathrm{m}}\| \leqslant \eta_{\mathrm{m}}\|\boldsymbol{y}_{\mathrm{m}}\|+\delta_{\mathrm{m}},\\ &0\leqslant\eta_{\mathrm{m}},\ \delta_{\mathrm{m}}<\infty,\ \boldsymbol{u}^*\in\mathcal{U}^*.\end{aligned} \tag{12}$$

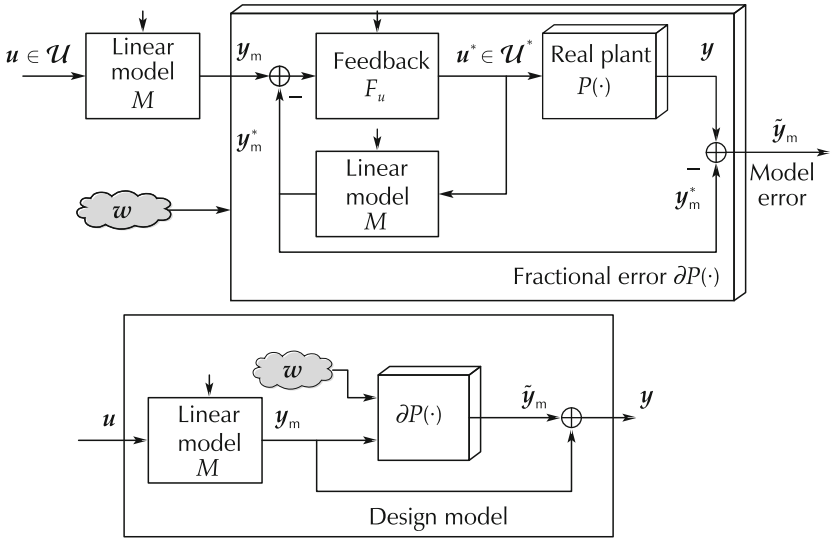

Fig. 1 Block diagram of the fractional error operator.

In the light of (4), an uncertainty defined by

$$\sigma_{\max}(\partial P(\mathrm{j}f)) \geqslant \eta > 1,\ \ f \geqslant f_{\partial P}, \tag{13}$$

and implying $\sigma_{\max}(V(\mathrm{j}f)) \leqslant 1/\eta < 1$, is such to contrast the sensitivity performance requirement $\sigma_{\max}(S(\mathrm{j}f)) \leqslant 1/\eta < 1$, $f \leqslant f_{\mathrm{s}}$, where $S = I - V$, as soon as $f_{\mathrm{s}} > f_{\partial P}$, leading to an unfeasible design.

Two questions arise. Which is the source of the in-

coherence among model, uncertainty and required performance? Focusing on the model and its uncertainty, is there a criterion for testing model adequacy?

F. Donati and M. Vallauri in [10] approached the problem by extending Kalman theory to robust design, i.e., by separating control strategies into state observer, feedback control law and reference generator. Under unstructured uncertainty, observer and control law design cease to be independent, but their dependence can be made sufficiently weak. Let the control performance be defined by the norm $\|W_r(\boldsymbol{r}-\boldsymbol{y})\|$ of the weighted tracking error $W_r(\boldsymbol{r}-\boldsymbol{y})$, where $\boldsymbol{r}\in\mathcal{R}$ is the reference signal belonging to a set $\mathcal{R}$ of the Hilbert space defined by (8) and W_r is a LP filter.

2.3.2 First design step: the almost-linear plant

The first design step is to look for an *almost-linear plant* $\hat{\boldsymbol{y}}=\hat{P}(\boldsymbol{u})$ with the following properties:

1) The unstructured uncertainty inequality, to be compared with (12), holds

$$\|\tilde{\boldsymbol{y}}\| = \|\hat{\boldsymbol{y}}-\boldsymbol{y}_m\| \leqslant \eta\|\boldsymbol{y}_m\|+\delta,\quad 0\leqslant\eta<1,\ 0\leqslant\delta<\infty,\ \boldsymbol{u}\in\mathcal{U}, \tag{14}$$

where $\tilde{\boldsymbol{y}}=\hat{\boldsymbol{y}}-\boldsymbol{y}_m$ is the model error of the almost-linear plant and $\eta<1$ in agreement with the small-gain theorem [11]. In (14) we took the liberty, justified by $T>\Delta t\geqslant 1/(2f_u)$, of assuming $\boldsymbol{y}_m=\boldsymbol{y}_m^*$ and $\boldsymbol{u}=\boldsymbol{u}^*$.

2) The norm $\|W_r(\boldsymbol{r}-\hat{\boldsymbol{y}})\|$ of the weighted tracking error $W_r(\boldsymbol{r}-\hat{\boldsymbol{y}})$ of the almost-linear plant, can be made arbitrarily small by the second design step in Section 2.3.3.

Real and almost linear plants are shown in Fig. 2.

The first property can be achieved by filtering the *open-loop model error* in (11), now rewritten as $\tilde{\boldsymbol{y}}_m=\boldsymbol{y}-\boldsymbol{y}_m$, through the CS $V_m=(I+MF_m)^{-1}MF_m$ of an AS state observer. The observer is built around M by means of a feedback operator F_m, which is driven by the *measured model error* $\boldsymbol{e}_m=\boldsymbol{y}-\hat{\boldsymbol{y}}$ (see the left-hand side (LHS) of Fig. 2). Controllability and observability of M are sufficient conditions for this design. Let us write $\hat{\boldsymbol{y}}$ in terms of the observer sensitivity $S_m=(I+MF_m)^{-1}$ and of the CS $V_m=I-S_m$, i.e.,

$$\hat{\boldsymbol{y}}=S_mMu+V_m\boldsymbol{y}\Rightarrow\hat{\boldsymbol{y}}-\boldsymbol{y}_m=V_m(\boldsymbol{y}-\boldsymbol{y}_m). \tag{15}$$

The right-hand side (RHS) identity of (15) allows the inequality (14) to be rewritten with the same variables of (12) as follows:

$$\|\tilde{\boldsymbol{y}}\| = \|\hat{\boldsymbol{y}}-\boldsymbol{y}_m\| = \|V_m\tilde{\boldsymbol{y}}_m\| \leqslant \eta\|\boldsymbol{y}_m\|+\delta,\quad 0\leqslant\eta<1,\ 0\leqslant\delta<\infty,\ \boldsymbol{u}\in\mathcal{U}. \tag{16}$$

Further, since V_m is a LP filter, (16) proves that an AS *state observer can attenuate the norm of the open-loop model error* $\tilde{\boldsymbol{y}}=\boldsymbol{y}-\boldsymbol{y}_m$ down to the norm of the almost-linear plant model error $\tilde{\boldsymbol{y}}$ (also *closed-loop model error* and *prediction error* in Section 3).

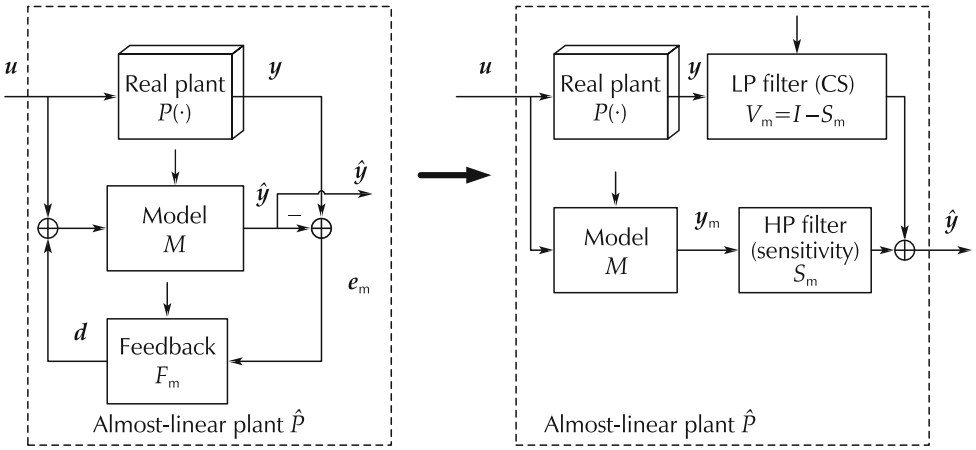

Fig. 2 Equivalence between a plant with a state observer and the almost-linear plant.

The LHS block-diagram in Fig. 2 shows plant and state observer, both driven by $\boldsymbol{u}$. Equation (15) allows us to draw the RHS diagram which shows how plant and model contribute to $\hat{P}$. For later use (see Section 3.1), the output $\boldsymbol{d}$ of the dynamic feedback F_m plays the role of an *input disturbance* adding to the command. This interpretation has been exploited by the EMC (see [7] and [11]) and by the Active Disturbance Rejection Control (ADRC) [3] in the design of F_m, with the aim of canceling the *unknown components* of $\boldsymbol{d}$ from the plant.

We also define the output disturbance

$$\boldsymbol{d}_y = M\boldsymbol{d}, \tag{17}$$

which is common in the classical control design. Thus, $\hat{P}$ can be rewritten as

$$\hat{\boldsymbol{y}} = M(\boldsymbol{u} + \boldsymbol{d}) = \boldsymbol{y}_{\mathrm{m}} + \boldsymbol{d}_y. \tag{18}$$

Since, given a controllable and observable M, a family of AS state observers with different filtering capabilities can be built, given a plant P, the design of an adequate model M is a *necessary condition* for the construction of an almost-linear plant satisfying (16). In other terms, given P and M, no V_{m} may exist that guarantees (16). The statement justifies Kalman's theory (the *modern control paradigm* in [3]) and contradicts the ubiquitous univariate PID feedback, whose design is substantially model independent and only guaranteed by the experimental performance of the measured tracking error $e(t)$, as pointed out by J. Han and Z. Gao in [1,3,6] (what they call the *error-based design paradigm*). The work of J. Han on the difficulties of the modern control paradigm in the real plant control design dates back to the 80's, but unfortunately his publications were restricted to Chinese language. He observed in [3] that the robust control design is a *paradox* that looks unsolvable within the modern control paradigm.

First of all, as pointed out by the same authors in [1] and [3], the ideal PID law

$$u(t) = k_{\mathrm{p}}e(t) + k_{\mathrm{i}}\int_0^t e(\tau)\mathrm{d}\tau + k_{\mathrm{d}}\frac{\mathrm{d}e(t)}{\mathrm{d}t} \tag{19}$$

cannot be implemented as it is, but the error e, its derivative $\dfrac{\mathrm{d}e}{\mathrm{d}t}$ and the reference signal must be arranged and adequately filtered to better match the simple feedback (19) with plant uncertainty and irregularities. Second, inequality (16) is a condition on the *fractional error operator* $\partial P(\boldsymbol{y}_{\mathrm{m}})$ defined in (11) and not on the model M. The second design step of the Donati-Vallauri's approach will prove that robust control design is concerned with the stability and performance of the so-called *error loop*, which was suggested by E. Canuto (2007) in [7] and again in [16] within the framework of the embedded model control. In essence, the argument of this paper is that almost-linear plant and error loop design can reconcile modern control and error-based control paradigms.

A first piece of the error loop is shown in Fig. 3, where model and tracking errors propagate along a closed loop. Section 2.3.3 will show that the stability of the error loop is a *necessary and sufficient condition* for the stability of the real closed-loop system. The loop is driven by the reference signal $\boldsymbol{r}$ and provides the *tracking error* in the form $\boldsymbol{r} - \boldsymbol{y}_{\mathrm{m}}$. The cloud driving the fractional error ∂P accounts for arbitrary and unpredictable sources of uncertainty (*causal uncertainty*) like the random measurement errors in the Kalman's theory. The block marked by "?" will be the result of the second design step.

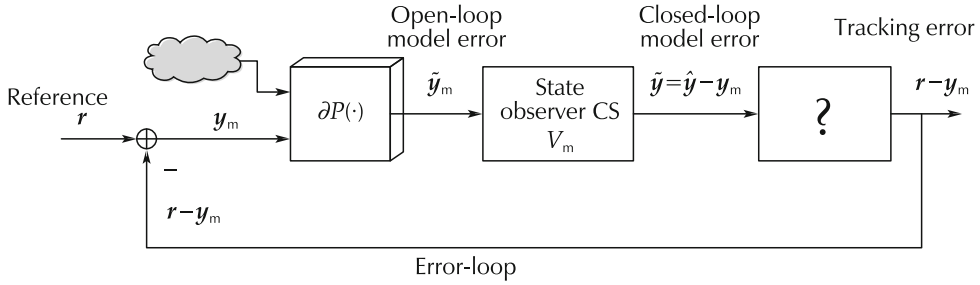

Fig. 3 A first piece of the error loop.

To conclude, since $\partial P(\cdot)$ is partially unknown and time-varying, inequality (16) cannot be exhaustively proved in the command set $\mathcal{U}$, given that the set $\partial\mathcal{P}$ of the candidate ∂P, though reasonably bounded, is partially unknown. This implies the risk that (16) ceases to be valid, the risk being commonly reduced, but not zeroed, by fixing a gain margin, that is $\eta \leqslant \eta_{\max} < 1$. The inverse $\eta_{\max}^{-1} > 1$ is known as the *gain margin*. Anomalous situations can be revealed by the controller itself and require an appropriate control system reconfiguration leading to degraded performance.

2.3.3 Second design step: fundamental theorem and error loop

Although (16) is a well-defined target for the observer design, it is *insufficient* for guaranteeing the closed-loop stability of an arbitrary *control law* around $\hat{P}$. This is reasonable, since the "small gain theorem" [11] requires

that the whole loop operator in Fig. 3 possesses a gain less than unit. In terms of the error loop in Fig. 3, we are still missing the operator mapping the closed-loop model error $\tilde{\boldsymbol{y}}$ into the tracking error $\boldsymbol{r} - \boldsymbol{y}_{\mathrm{m}}$.

The control requirement is formulated by the norm inequality

$$\|W_{\mathrm{r}}(\boldsymbol{r} - \boldsymbol{y})\| \leqslant \eta_{\mathrm{r}}\|\boldsymbol{r}\| + \delta_{\mathrm{r}},\ 0 \leqslant \eta_{\mathrm{r}},\ \delta_{\mathrm{r}} < \infty,\ \boldsymbol{r} \in \mathcal{R}, \quad (20)$$

where W_{r} is a LP filter that was already defined and $\mathcal{R}$ is the reference signal set. The feedback design around $\hat{P}$ requires that $\hat{\boldsymbol{y}}$ appears in (20), which is obtained with the help of (15) and by splitting the weighted tracking error as

$$\begin{aligned} W_{\mathrm{r}}(\boldsymbol{r} - \boldsymbol{y}) &= W_{\mathrm{r}}(\boldsymbol{r} - \hat{\boldsymbol{y}} + \hat{\boldsymbol{y}} - \boldsymbol{y}) \\ &= W_{\mathrm{r}}(\boldsymbol{r} - \hat{\boldsymbol{y}}) - W_{\mathrm{r}}S_{\mathrm{m}}(\boldsymbol{y} - \boldsymbol{y}_{\mathrm{m}}), \end{aligned} \quad (21)$$

where $W_{\mathrm{r}}(\boldsymbol{r} - \hat{\boldsymbol{y}})$ is the weighted tracking error of $\hat{P}$ and $\boldsymbol{y} - \hat{\boldsymbol{y}} = W_{\mathrm{r}}S_{\mathrm{m}}(\boldsymbol{y} - \boldsymbol{y}_{\mathrm{m}})$ is the open-loop model error filtered by the band-pass filter $W_{\mathrm{r}}S_{\mathrm{m}}$. The mid-frequency error $\boldsymbol{y} - \hat{\boldsymbol{y}}$ may be referred to as the *residual model error* since free of low-frequency (LF) components (they are eliminated by S_{m}) and HF components (they are eliminated by W_{r}). In general, the residual model error cannot be brought to zero, since the frequency BW of W_{r} is wider than that of S_{m}.

We now state the *fundamental theorem*, which proves the second property of almost-linear plants and justifies their construction.

Fundamental design theorem The tracking error norm $\|W_{\mathrm{r}}(\boldsymbol{r} - \hat{\boldsymbol{y}})\|$ can be made arbitrarily small by the control law

$$\boldsymbol{u} = C(\boldsymbol{r} - \hat{\boldsymbol{y}}) + C_{\mathrm{r}}\boldsymbol{r}, \quad (22)$$

which is applied to the almost-linear plant defined by (18) under the sufficient conditions:

$$\begin{cases} \eta\|V_{\mathrm{c}}\|_\infty < 1, \\ \|W_{\mathrm{r}}S_{\mathrm{c}}\|_\infty \to 0, \\ MC_{\mathrm{r}} = I, \end{cases} \quad (23)$$

where $V_{\mathrm{c}}(z) = I - S_{\mathrm{c}}(z)$ is the CS of $S_{\mathrm{c}} = (I + MC)^{-1}$.

The first condition states that the loop gain $\eta\|V_{\mathrm{c}}\|_\infty$ must be less than unit (*bounded-input-bounded-output stable closed loop*); the second condition states that the gain of the band-pass filter $W_{\mathrm{r}}S_{\mathrm{c}}$ can be made arbitrarily small by enlarging the frequency BW of S_{c} (*efficient closed-loop control*); the third condition fixes the reference gain in (22). The first and second condition are each other contrasting, but the contrast is attenuated by $\eta < 1$ as required by the almost-linear plant design in (16). More practical is the lower bound $\|W_{\mathrm{r}}S_{\mathrm{c}}\|_\infty \geqslant \varepsilon_{\mathrm{r}}$, which is imposed by the command set $\mathcal{U}$ (typically $|\boldsymbol{u}(t)| \leqslant u_{\max}$) and in general by technology limitations and cost. EMC exploits these and other contrasting inequalities by generating frequency bands where the bandwidths of the state observer and control law sensitivity, and of their CS, are compelled to stay. When these regions become void, they reveal that the control requirement in (20) cannot be met. The third condition cannot be exactly met, but can be approximated by a wide-band closed-loop inverse $C_{\mathrm{r}} = V_{\mathrm{r}}M^{-1}$ like in (10). Fig. 4 shows the overall closed-loop system which consists of the almost-linear plant in Fig. 2 and of the control law (22).

Before completing the error loop in Fig. 3, we need to prove the fundamental theorem.

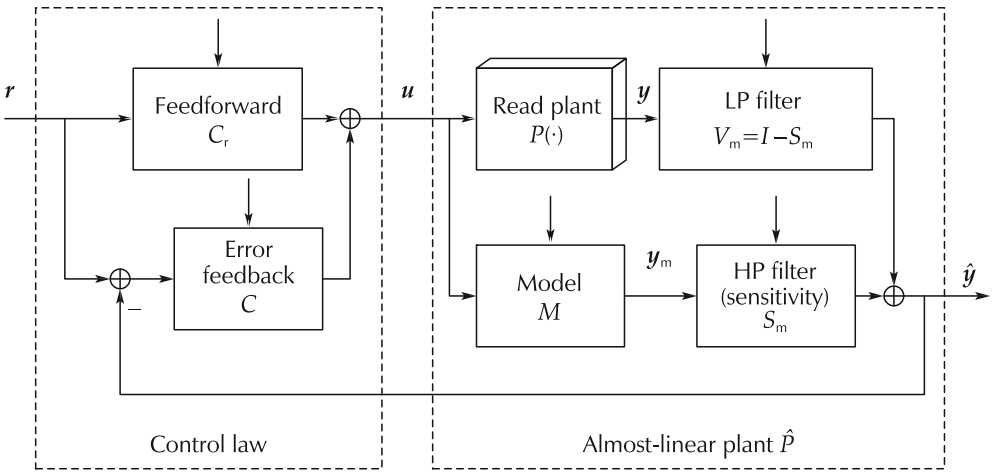

Fig. 4 The closed-loop system.

Proof of the fundamental theorem The proof starts by replacing (22) into (18), which provides

$$\hat{\boldsymbol{y}} = MC(\boldsymbol{r} - \hat{\boldsymbol{y}}) + MC_{\mathrm{r}}\boldsymbol{r} + M\boldsymbol{d}. \tag{24}$$

By using the third condition in (23), we obtain the pair of identities

$$\begin{cases} \boldsymbol{r} - \hat{\boldsymbol{y}} = S_{\mathrm{c}}(I - MC_{\mathrm{r}})\boldsymbol{r} - S_{\mathrm{c}}\boldsymbol{d}_y = -S_{\mathrm{c}}(\hat{\boldsymbol{y}} - \boldsymbol{y}_{\mathrm{m}}), \\ \boldsymbol{r} - \boldsymbol{y}_{\mathrm{m}} = (\hat{\boldsymbol{y}} - \boldsymbol{y}_{\mathrm{m}}) + (\boldsymbol{r} - \hat{\boldsymbol{y}}) = V_{\mathrm{c}}(\hat{\boldsymbol{y}} - \boldsymbol{y}_{\mathrm{m}}), \end{cases} \tag{25}$$

and the pair of inequalities

$$\begin{cases} \|W_{\mathrm{r}}(\boldsymbol{r} - \hat{y})\| \leqslant \|W_{\mathrm{r}}S_{\mathrm{c}}\|_\infty \|\hat{\boldsymbol{y}} - \boldsymbol{y}_{\mathrm{m}}\|, \\ \|\boldsymbol{y}_{\mathrm{m}}\| \leqslant \|\boldsymbol{r}\| + \|V_{\mathrm{c}}\|_\infty \|\hat{\boldsymbol{y}} - \boldsymbol{y}_{\mathrm{m}}\|. \end{cases} \tag{26}$$

Replacement of the second inequality of (26) into (16) allows the closed-loop model error $\tilde{\boldsymbol{y}} = \hat{\boldsymbol{y}} - \boldsymbol{y}_{\mathrm{m}}$ to be expressed in terms of $\boldsymbol{r}$ as follows:

$$\begin{aligned} \|\tilde{\boldsymbol{y}}\| = \|\hat{\boldsymbol{y}} - \boldsymbol{y}_{\mathrm{m}}\| &\leqslant \eta\|\boldsymbol{y}_{\mathrm{m}}\| + \delta \\ &\leqslant \eta\|\boldsymbol{r}\| + \eta\|V_{\mathrm{c}}\|_\infty \|\hat{\boldsymbol{y}} - \boldsymbol{y}_{\mathrm{m}}\| + \delta \\ \Rightarrow \|\tilde{\boldsymbol{y}}\| &\leqslant (1 - \eta\|V_{\mathrm{c}}\|_\infty)^{-1}(\eta\|\boldsymbol{r}\| + \delta). \end{aligned} \tag{27}$$

Finally, replacement of the third row of (27) into the first row of (26) provides the expected inequality:

$$\|W_{\mathrm{r}}(\boldsymbol{r} - \hat{\boldsymbol{y}})\| \leqslant \frac{\|W_{\mathrm{r}}S_{\mathrm{c}}\|_\infty(\eta\|\boldsymbol{r}\| + \delta)}{1 - \eta\|V_{\mathrm{c}}\|_\infty} = \hat{\eta}\|\boldsymbol{r}\| + \hat{\delta}, \tag{28}$$

which is *bounded* under the first condition of (23) and *converges to zero* under the second condition. □

The error loop in Fig. 3 is ready to be completed. The last row of (25) provides the missing operator, the CS V_{c}, which completes the error loop as in Fig. 3. Three tracking errors are at the output of the error loop: $\boldsymbol{r} - \boldsymbol{y}$ (from the real plant) and $\boldsymbol{r} - \hat{\boldsymbol{y}}$ (from the almost-linear plant) already appeared in the decomposition of (21), whereas $\boldsymbol{r} - \boldsymbol{y}_{\mathrm{m}}$ (from the model) appeared in the second row of (25). Error loop stability can be defined as follows.

Error loop stability The error loop in Fig. 5 is bounded-input-bounded-output stable if for any bounded $\boldsymbol{r} \in \mathcal{R}$ all the error loop signals are bounded.

A sufficient stability condition is that

$$\begin{cases} \|\boldsymbol{r} - \boldsymbol{y}_{\mathrm{m}}\| \leqslant \eta_{\mathrm{e}}\|\boldsymbol{y}_{\mathrm{m}}\| + \delta_{\mathrm{e}}, \\ 0 \leqslant \eta_{\mathrm{e}} = \eta\|V_{\mathrm{c}}\|_\infty < 1,\ 0 \leqslant \delta_{\mathrm{e}} < \infty, \end{cases} \tag{29}$$

since it implies that $\|\boldsymbol{y}_{\mathrm{m}}\|$ and all the other loop signals are bounded. To prove it, consider the following upper bound of $\|\boldsymbol{y}_{\mathrm{m}}\|$:

$$\begin{cases} \|\boldsymbol{y}_{\mathrm{m}}\| = \|\boldsymbol{r} - \boldsymbol{r} + \boldsymbol{y}_{\mathrm{m}}\| \leqslant \|\boldsymbol{r}\| + \eta_{\mathrm{e}}\|\boldsymbol{y}_{\mathrm{m}}\| + \delta_{\mathrm{e}}, \\ \|\boldsymbol{y}_{\mathrm{m}}\| \leqslant (1 - \eta_{\mathrm{e}})^{-1}(\|\boldsymbol{r}\| + \delta_{\mathrm{e}}), \end{cases} \tag{30}$$

which, being $\|\boldsymbol{r}\|$ bounded inside $\mathcal{R}$, is bounded under $\eta_{\mathrm{e}} < 1$. The identity $\eta_{\mathrm{e}} = \eta\|V_{\mathrm{c}}\|_\infty$ follows from the almost-linear plant inequality (14) and the last row of (25) (see also Fig. 5).

We now prove that the error loop stability is necessary and sufficient for the closed-loop plant stability. To this end, let us observe that the extraction of the tracking error $\boldsymbol{r} - \boldsymbol{y}$ as in Fig. 5 converts the error loop into the closed-loop plant from $\boldsymbol{r}$ to $\boldsymbol{r} - \boldsymbol{y}$. The closed-loop plant stability can be defined as in (7) (finite-gain stability). A finite non-negative pair $\{\eta_{\mathrm{c}}, \delta_{\mathrm{c}}\}$ must exist such that

$$\|\boldsymbol{r} - \boldsymbol{y}\| \leqslant \eta_{\mathrm{c}}\|\boldsymbol{r}\| + \delta_{\mathrm{c}},\ \ 0 \leqslant \eta_{\mathrm{c}} < \infty,\ 0 \leqslant \delta_{\mathrm{c}} < \infty. \tag{31}$$

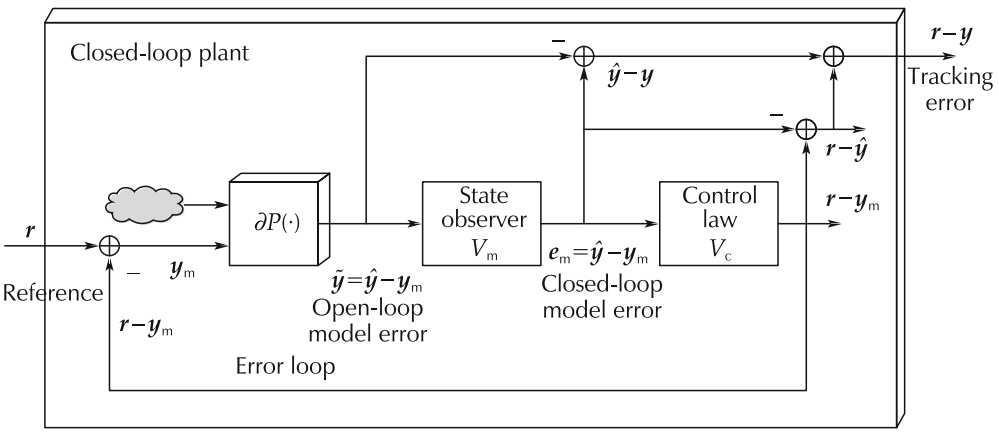

Fig. 5 The error loop and the closed-loop plant.

Closed-loop plant stability theorem Consider a plant $\boldsymbol{y} = P(\boldsymbol{u})$ with $\boldsymbol{u} \in \mathcal{U}$ and a minimal LTI model $\boldsymbol{y}_\mathrm{m} = M\boldsymbol{u}$. Model minimality implies that a class of asymptotically stable CS V_m and V_c exists for the state observer and the control law. Let us define the reference set $\boldsymbol{r} \in \mathcal{R}$, the fractional model error $\partial P(\boldsymbol{y}_\mathrm{m})$ as in (11) and the corresponding error loop as in Fig. 5. The stability of the error loop defined by (29) is a necessary and sufficient condition for the closed-loop plant stability defined by (31).

Proof (Sufficient condition: error loop stability implies closed-loop plant stability) Let us write the norm of the plant tracking error $\boldsymbol{r} - \boldsymbol{y}$ in terms of the components of the error loop in Fig. 5:

$$\|\boldsymbol{r} - \boldsymbol{y}\| \leqslant \|\boldsymbol{r} - \boldsymbol{y}_\mathrm{m}\| + \|\boldsymbol{y}_\mathrm{m} - \boldsymbol{y}\|. \tag{32}$$

From (12), (29) and (30), and by setting $\boldsymbol{y}^*_\mathrm{m} = \boldsymbol{y}_\mathrm{m}$ and $\boldsymbol{u}^* = \boldsymbol{u}$ in (12), we obtain

$$\begin{aligned}
&\|\boldsymbol{r} - \boldsymbol{y}\| \\
&\leqslant (\eta_\mathrm{e} + \eta_\mathrm{m})\|\boldsymbol{y}_\mathrm{m}\| + \delta_\mathrm{m} + \delta_\mathrm{e} \\
&\leqslant (\eta_\mathrm{e} + \eta_\mathrm{m})(1 - \eta_\mathrm{e})^{-1}\|\boldsymbol{r}\| + \delta_\mathrm{m} + (1 + \frac{\eta_\mathrm{e} + \eta_\mathrm{m}}{1 - \eta_\mathrm{e}})\delta_\mathrm{e} \\
&\leqslant \eta_\mathrm{c}\|\boldsymbol{r}\| + \delta_\mathrm{c},
\end{aligned} \tag{33}$$

where, because of $\eta_\mathrm{e} < 1$, we find, as required, that

$$\begin{cases}
0 \leqslant \eta_\mathrm{c} = \dfrac{\eta_\mathrm{e} + \eta_\mathrm{m}}{1 - \eta_\mathrm{e}} < \infty, \\
0 \leqslant \delta_\mathrm{c} = \delta_\mathrm{m} + (1 + \dfrac{\eta_\mathrm{e} + \eta_\mathrm{m}}{1 - \eta_\mathrm{e}})\delta_\mathrm{e} < \infty.
\end{cases} \tag{34}$$

Furthermore, $\|\boldsymbol{r}\|$ is bounded and thus proves (31) and sufficiency.

(Necessary condition: closed-loop plant stability implies error loop stability) Now let us assume (31). Let us decompose $\boldsymbol{r} - \boldsymbol{y}_\mathrm{m}$ as follows:

$$\boldsymbol{r} - \boldsymbol{y}_\mathrm{m} = (\boldsymbol{r} - \boldsymbol{y}) - (\boldsymbol{r} - \boldsymbol{y}) + V_\mathrm{c}(\hat{\boldsymbol{y}} - \boldsymbol{y}_\mathrm{m}). \tag{35}$$

The last equation, with the help of (16), converts into the norm inequality

$$\begin{aligned}
\|\boldsymbol{r} - \boldsymbol{y}_\mathrm{m}\| &\leqslant 2\|\boldsymbol{r} - \boldsymbol{y}\| + \|V_\mathrm{c}\|_\infty\|\hat{\boldsymbol{y}} - \boldsymbol{y}_\mathrm{m}\| \\
&\leqslant \eta\|V_\mathrm{c}\|_\infty\|\boldsymbol{r} - \boldsymbol{y}_\mathrm{m}\| \\
&\quad +(2\eta_\mathrm{c} + \eta)\|\boldsymbol{r}\| + 2\delta_\mathrm{c} + \delta
\end{aligned} \tag{36}$$

with $\eta < 1$, and finally, into the inequality

$$\|\boldsymbol{r} - \boldsymbol{y}_\mathrm{m}\| \leqslant (1 - \eta\|V_\mathrm{c}\|_\infty)^{-1}((2\eta_\mathrm{c} + \eta)\|\boldsymbol{r}\| + 2\delta_\mathrm{c} + \delta) \tag{37}$$

with $\eta < 1$. For $\|\boldsymbol{r} - \boldsymbol{y}_\mathrm{m}\|$ to be bounded, the last inequality requires that $\eta\|V_\mathrm{c}\|_\infty < 1$ as in the stability condition (29) of the error loop. □

The theorem is believed to reconcile *modern control theory* with the *error-based control design*. In fact, from one side, given the minimal LTI model M, a class of AS CS V_m (state observer) and V_c (control law) can be designed and optimal elements singled out. On the other hand, robust performance versus uncertainty can *only* be guaranteed by the *error loop*, which converts $\boldsymbol{r}$ into the set $\{\boldsymbol{r} - \boldsymbol{y}, \boldsymbol{r} - \hat{\boldsymbol{y}}, \boldsymbol{r} - \boldsymbol{y}_\mathrm{m}\}$ of tracking errors passing through the unstructured uncertainty, which has been written in the fractional form $\partial P(\cdot)$. The uncertainty attenuation is made possible by dynamic operators designed within the modern control theory.

2.3.4 Approximate separation between almost-linear plant and control law design

The fundamental theorem can be employed by constraining the tracking error norm $\|W_\mathrm{r}(\hat{\boldsymbol{y}} - \boldsymbol{r})\|$ of $\hat{P}$ to be negligible with respect to the control requirements, i.e.,

$$\begin{cases}
(1 - \eta\|V_\mathrm{c}\|_\infty)^{-1}\|W_\mathrm{r}S_\mathrm{c}\|_\infty\eta \ll \eta_\mathrm{r}, \\
(1 - \eta\|V_\mathrm{c}\|_\infty)^{-1}\|W_\mathrm{r}S_\mathrm{c}\|_\infty\delta \ll \delta_\mathrm{r}.
\end{cases} \tag{38}$$

This implies that the requirement in (20) simplifies into

$$\|W_\mathrm{r}S_\mathrm{m}(\boldsymbol{y} - \boldsymbol{y}_\mathrm{m})\| \leqslant \eta_\mathrm{r}\|\boldsymbol{r}\| + \delta_\mathrm{r}. \tag{39}$$

Inequality (39) when combined with (14) establishes a pair of inequalities for the design of the *almost-linear plant* $\hat{P}$, i.e., of the state observer which consists of the *model* M and of the *feedback* F_m. To this end, with the help of (26) and (27), (14) is rewritten in terms of $\boldsymbol{r}$ as follows:

$$\begin{aligned}
\|\tilde{\boldsymbol{y}}\| &= \|V_\mathrm{m}(\boldsymbol{y} - \boldsymbol{y}_\mathrm{m})\| \\
&\leqslant \eta(1 + \alpha(\cdot))\|\boldsymbol{r}\| + \delta(1 + \frac{\alpha(\cdot)}{\eta}),
\end{aligned} \tag{40}$$

where $\eta < 1$ and the correction $\alpha(\cdot) = \eta\|V_\mathrm{c}\|_\infty(1 - \eta\|V_\mathrm{c}\|_\infty)^{-1} = \mathrm{o}(\eta\|V_\mathrm{c}\|_\infty)$, being of the order of $\eta\|V_\mathrm{c}\|_\infty$, depends on the control-law design.

It looks natural to derive the following *approximate separation* in the presence of the unstructured uncertainty:

1) *Uncertainty-based design*: given the control requirements collected in $\{\eta_\mathrm{r}, \delta_\mathrm{r}, W_\mathrm{r}, \boldsymbol{r} \in \mathcal{R}\}$, the plant $\{\boldsymbol{y} = P(\boldsymbol{u}), \boldsymbol{u} \in \mathcal{U}\}$ and a first guess $V_{\mathrm{c}0}$ of V_c, M and F_m are designed to satisfy (39) and (40).

2) *Model-based design*: given $\{\eta_r, \delta_r, W_r, \boldsymbol{r} \in \mathcal{R}\}$, the model M and the technology constraint $\|W_r S_c\| \geqslant \varepsilon_r$, the pair $\{C, C_r\}$ in (24) is designed to satisfy the third condition in (23) and (38).

3) Iteration. Given V_{ck}, $k \geqslant 1$, the above design steps are repeated until all the design inequalities (38), (39) and (40) are satisfied.

3 The path toward embedded model control

Embedded model control is an extension of the Donati-Vallauri's theory outlined in Section 2.3. The aim is an analytic design and an implementation method, both centered on the DT state equations of the *embedded model*.

3.1 First design step: embedded and design model, uncertainty and state predictor

The embedded model is an extension of the LTI model M in Fig. 1. It includes the dynamics D of the feedback F_m in Fig. 2, which generates the input disturbance $\boldsymbol{d}$ in (17) from a vector $\boldsymbol{w}$ of arbitrary (hence uncorrelated), bounded and unbiased signals. If $\boldsymbol{w}$ is given the stochastic meaning of a zero-mean bounded-variance white noise process with constant power spectral density (PSD) S_w^2 and $D(s)$ is a transfer matrix, the PSD $S_d^2(f)$ of $\boldsymbol{d}$ can be factored as

$$S_d^2(f) = D(\mathrm{j}f) S_w^2 D^T(-\mathrm{j}f). \tag{41}$$

Therefore, as in [11], the embedded model is the composition of the controllable command-to-output dynamics M with state $\boldsymbol{x}_c$ and of the disturbance dynamics D with state $\boldsymbol{x}_d$. Given the time unit T and the Nyquist frequency $f_{max} = 0.5/T$, the standard embedded model is written as follows:

$$\begin{cases} \begin{bmatrix} \hat{\boldsymbol{x}}_c \\ \hat{\boldsymbol{x}}_d \end{bmatrix}(i+1) = \begin{bmatrix} A_c & H_c \\ 0 & A_d \end{bmatrix} \begin{bmatrix} \hat{\boldsymbol{x}}_c \\ \hat{\boldsymbol{x}}_d \end{bmatrix} + \begin{bmatrix} B_c \\ 0 \end{bmatrix} (\boldsymbol{u} + \underline{\boldsymbol{h}}(\cdot)) \\ \qquad\qquad + \begin{bmatrix} G_c & 0 \\ 0 & G_d \end{bmatrix} \widehat{\boldsymbol{w}}, \\ \hat{\boldsymbol{y}}(i) = [C_c \;\; C_d] \begin{bmatrix} \hat{\boldsymbol{x}}_c \\ \hat{\boldsymbol{x}}_d \end{bmatrix}, \end{cases} \tag{42}$$

where initial conditions and time i have been omitted, the inline vector notation of [11] allows us to write $\widehat{\boldsymbol{w}} = [\widehat{\boldsymbol{w}}_c, \widehat{\boldsymbol{w}}_d]$, the sub-matrices, the nonlinear term $\underline{\boldsymbol{h}}(\cdot) = \underline{\boldsymbol{h}}(\hat{\boldsymbol{x}}_c)$ and the initial state are known, and the command $\boldsymbol{u}$ is the same dispatched to the plant. The state vector $\hat{\boldsymbol{x}} = [\hat{\boldsymbol{x}}_c, \hat{\boldsymbol{x}}_d]$ (inline notation) is observable from $\hat{\boldsymbol{y}}$ and $\hat{\boldsymbol{x}}_c$ is controllable by $\boldsymbol{u}$. In the simplest case, $\hat{\boldsymbol{x}}$ is controllable by $\widehat{\boldsymbol{w}}$, where the inverted breve " $\widehat{\ }$ " signifies estimate, and the caret "ˆ" signifies one-step prediction.

Of the four uncertainty classes in [11], namely, causal and parametric uncertainty, initial state and neglected dynamics, (42) only retains the *causal uncertainty* expressed by $\widehat{\boldsymbol{w}}$. The other three classes are expressed with the help of the *design model*, which surrogates the plant P of Section 2.3. The design model output is $\boldsymbol{y}$ (the plant output) and the state is the vector $\boldsymbol{x} = [\boldsymbol{x}_c, \boldsymbol{x}_d]$, which is the homologous of $\hat{\boldsymbol{x}}$ in (42) and plays the role of the *true state*. The *parametric uncertainty*, not treated in Section 2.3, is the difference $\Delta\boldsymbol{h} = \boldsymbol{h}(\boldsymbol{x}_c) - \underline{\boldsymbol{h}}(\hat{\boldsymbol{x}}_c)$ with respect to the design-model term $\boldsymbol{h}(\boldsymbol{x}_c)$. The *initial state uncertainty* $\tilde{\boldsymbol{x}}_0 = \boldsymbol{x}_0 - \hat{\boldsymbol{x}}_0$ defines the initial prediction error. The *fractional error operator* ∂P of the neglected dynamics is defined as in (11), by decomposing $\boldsymbol{y}$ as follows:

$$\begin{aligned} \boldsymbol{y}(t) &= \boldsymbol{y}_m(t) + \tilde{\boldsymbol{y}}_m(t) \\ &= \boldsymbol{y}_m(t) + \partial P(\boldsymbol{y}_m) + \boldsymbol{w}_m(t), \end{aligned} \tag{43}$$

where $\boldsymbol{y}_m$ is the homologous of $\hat{\boldsymbol{y}}$ in (42) and plays the role of the model output of the design model. Finally, $\boldsymbol{w}_m$ is the random measurement error (absent in Section 2.3). ∂P is here approximated by a linear operator represented by the transfer matrix $\partial P(s)$. Some properties of $\partial P(s)$ can be found in [11]. The case study in Section 4 will point out an unstable $\partial P(s)$ not treated in [11]. The input disturbance $\boldsymbol{d}$ in (17) is now a signal of the design model and holds

$$\boldsymbol{d} = H_c \boldsymbol{x}_d + \boldsymbol{h}(\boldsymbol{x}_c) + G_c \boldsymbol{w}_c, \tag{44}$$

where $\boldsymbol{w}_c$ is not marked to signify the uncertainty class of the design model.

Separation between parametric uncertainty and neglected dynamics is a design issue as pointed out in [17]. As a rule, $\Delta\boldsymbol{h}$ does not add any dynamics to the model, but describes nonlinear terms, cross-coupling and parametric uncertainty to be rejected. On the contrary, ∂P accounts for short-term additional dynamics (delay, resonance, partial differential equations) whose contribution to $\boldsymbol{y}$ must be blocked from spilling into embedded model and control law. This is the goal of the *noise estimator* $\widehat{\boldsymbol{w}}(z) = N(z)(\boldsymbol{y} - \hat{\boldsymbol{y}})(z)$, which implies that the feedback F_m of Fig. 2 is factorized as $F_m(z) = D(z)N(z)$.

If G_c is not full rank (but G_d can be designed to be full rank), two singular cases may occur as in Section 4.

1) State derivatives close to the output $\hat{\boldsymbol{y}}$ are noise free, like the point-mass velocity (the same applies to the tank level rate in Section 4). In this event, a static output-to-noise feedback N cannot stabilize the embedded model and must be replaced by a dynamic feedback. However, a static N may be employed, if a measurement of the noise-free state derivatives is made available as in navigation problems (see [11] and [18]).

2) State derivatives close to the model command $\boldsymbol{u}$ are noise free like in Section 4, where the plant command is the integral of model command $\boldsymbol{u}$. In this case, the relevant states are stabilized by the control law and not by N.

The design of the sub-matrices $\{H_c, G_c, A_d, G_d\}$ and of N, which has been referred to as the noise design in [19], aims to distribute the necessary and sufficient uncertainty input points to the embedded model. The generic state equation of N is the following:

$$\begin{cases} \boldsymbol{x}_e(i+1) = A_e\boldsymbol{x}_e(i) + \boldsymbol{y}(i) - \hat{\boldsymbol{y}}(i), \\ \begin{bmatrix} \widehat{\boldsymbol{w}}_c \\ \widehat{\boldsymbol{w}}_d \end{bmatrix}(i) = \begin{bmatrix} N_c \\ N_d \end{bmatrix}\boldsymbol{x}_e + \begin{bmatrix} L_c \\ L_d \end{bmatrix}(\boldsymbol{y} - \hat{\boldsymbol{y}}), \end{cases} \tag{45}$$

where i has been partly omitted. The equation pair that consists of (42) and (45) constitutes a *state predictor* (SP), which replaces the *almost linear plant* of Section 2.3. The term state predictor is preferable to state observer since (42) naturally provides the state one-step prediction. The quintuple of matrices $\{L_c, L_d, N_c, N_d, A_e\}$ must be designed to stabilize the SP complementary spectrum $\Gamma_m = \{\gamma_{mj}\}$, with $\gamma_{mj} = 1 - \lambda_{mj}$, $j = 1, \ldots, n_m$ (pole placement). The size n_e of $\boldsymbol{x}_e$ depends on rank G_c.

If we assume that $\boldsymbol{h}(\boldsymbol{x}_c)$ is unknown (in other terms $\underline{\boldsymbol{h}}(\hat{\boldsymbol{x}}_c) = 0$ in (42)), the Z-transform of the output prediction error $\tilde{\boldsymbol{y}} = \hat{\boldsymbol{y}} - \boldsymbol{y}_m$ can be proved as in [11] to satisfy the *design equation*

$$\tilde{\boldsymbol{y}}(z) = V_m(z, \Gamma_m)\tilde{\boldsymbol{y}}_m(z) - S_m(z, \Gamma_m)\boldsymbol{d}_y(z), \tag{46}$$

where the pair $\{S_m, V_m\}$, which has been already employed in (15) is a function of Γ_m, $\tilde{\boldsymbol{y}}_m$ is the model error defined in (11) and (43), and $\boldsymbol{d}_y$ is the output disturbance defined in (17). The identity in (46) becomes the first part of the control unit in Fig. 6, where the EMC error loop is drawn.

In a more detailed way than the normed inequality (16), (46) distinguishes between two sets of uncertainty contributing to $\tilde{\boldsymbol{y}}$:

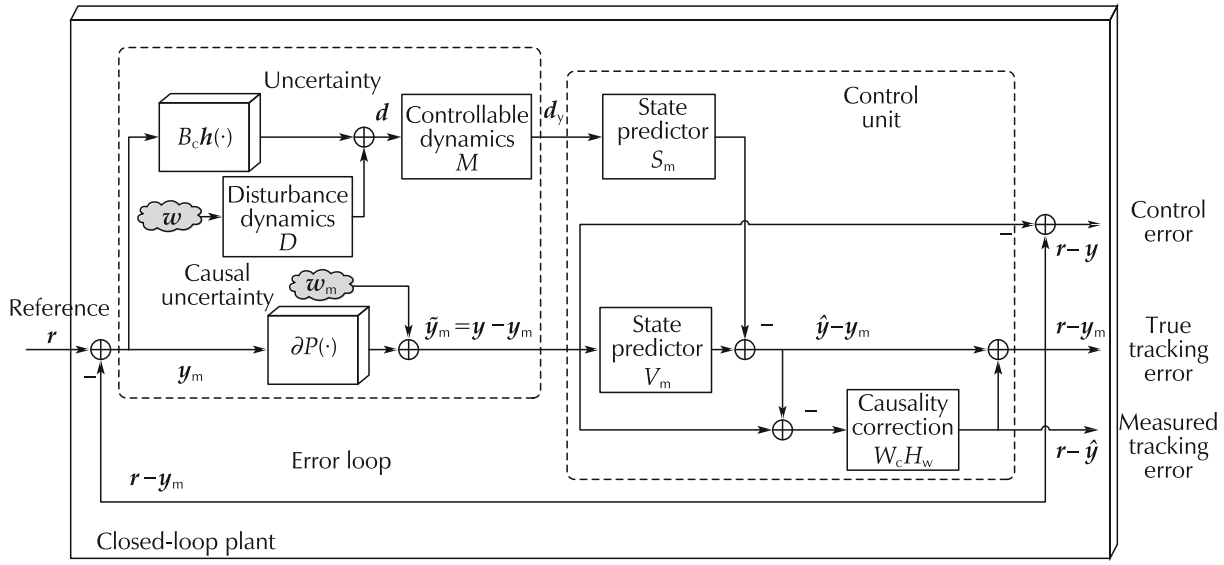

Fig. 6 The error loop according to embedded model control.

1) The first one is the uncertainty depending on $\boldsymbol{y}_m$ like the output of the fractional error $\partial P(\boldsymbol{y}_m)$ in (43) and $\boldsymbol{h}(\boldsymbol{x}_c)$ in (44). Their bounded uncertainty sets $\partial P(\cdot, \boldsymbol{p}) \in \partial\mathcal{P}$ and $\boldsymbol{h}(\cdot, \boldsymbol{p}) \in \mathcal{H}$ are parameterized by a bounded set $\boldsymbol{p} \in \Pi$ of parameters.

2) The second one is the uncertainty which is independent of $\boldsymbol{y}_m$ like $\boldsymbol{w}_m$ in (43) and $H_c\boldsymbol{x}_d + G_c\boldsymbol{w}_c$ in (44). Their uncertainty sets can be defined by their bounded PSD, $S^2_{\boldsymbol{w}m}(f)$ of $\boldsymbol{w}_m$ and $S^2_{\boldsymbol{w}}(f)$ of $\boldsymbol{w} = [\boldsymbol{w}_c, \boldsymbol{w}_d]$, which has been already employed in (41).

Given a norm requirement on $\tilde{\boldsymbol{y}}$ and the above uncertainty sets, the first design step is to find the SP spectrum Γ_{m}, which guarantees that $\tilde{\boldsymbol{y}}$ is bounded (stability) and satisfies the norm requirement (accuracy). Since as shown by (40), this step weakly depends on the control law design, and control requirements are in terms of the tracking error $\tilde{\boldsymbol{y}}_{\mathrm{r}}$, we omit the SP design step, and in Section 3.2 we just treat the combined pole placement of $\Gamma = \{\Gamma_{\mathrm{m}}, \Gamma_{\mathrm{c}}\}$, where Γ_{c} is the control-law spectrum.

3.2 Second design steps: control law and tracking error

As a control performance, the prediction error in (46) must be replaced by the *true output tracking error* $\tilde{\boldsymbol{y}}_{\mathrm{r}} = \boldsymbol{r} - \boldsymbol{y}_{\mathrm{m}}$, not to be confused with the classical control error $\boldsymbol{r} - \boldsymbol{y}$. The output error is related to the measured tracking error $\boldsymbol{e}_{\mathrm{r}}$ of the control law as follows:

$$\begin{cases} \tilde{\boldsymbol{y}}_{\mathrm{r}} = C_{\mathrm{c}}(\boldsymbol{x}_{\mathrm{c}} - \boldsymbol{x}_{\mathrm{r}}) = C_{\mathrm{c}}(\boldsymbol{x}_{\mathrm{c}} - \hat{\boldsymbol{x}}_{\mathrm{c}}) - C_{\mathrm{d}}\hat{\boldsymbol{x}}_{\mathrm{d}} + C_{\mathrm{c}}\boldsymbol{e}_{\mathrm{r}}, \\ \boldsymbol{e}_{\mathrm{r}} = \hat{\boldsymbol{x}}_{\mathrm{c}} - \boldsymbol{x}_{\mathrm{r}} + Q\hat{\boldsymbol{x}}_{\mathrm{d}}. \end{cases} \tag{47}$$

Equation (47) assumes the matrix identity $C_{\mathrm{d}} = C_{\mathrm{c}}Q$, which is part of the Davison-Francis equation [11]

$$\begin{bmatrix} H_{\mathrm{c}} + QA_{\mathrm{d}} \\ C_{\mathrm{d}} \end{bmatrix} = \begin{bmatrix} A_{\mathrm{c}} & B_{\mathrm{c}} \\ C_{\mathrm{c}} & 0 \end{bmatrix} \begin{bmatrix} Q \\ P \end{bmatrix}. \tag{48}$$

Equation (48) fixes the disturbance rejection matrices Q and P of the control law

$$\boldsymbol{u}(i) = \boldsymbol{u}_{\mathrm{r}}(i) - (K\boldsymbol{e}_{\mathrm{r}}(i) + P\hat{\boldsymbol{x}}_{\mathrm{d}}(i)), \tag{49}$$

where $\boldsymbol{u}_{\mathrm{r}}$ is the reference command, which satisfies the controllable dynamics, and the feedback matrix K stabilizes the complementary spectrum $\Gamma_{\mathrm{c}} = \{\gamma_{cj}\}$, $j = 1, \ldots, n_{\mathrm{c}}$ of $A_{\mathrm{c}} - B_{\mathrm{c}}K$.

In [11], the Z-transform of $\tilde{\boldsymbol{y}}_{\mathrm{r}}$ has been proved to satisfy a similar equation to (46), namely:

$$\begin{cases} \tilde{\boldsymbol{y}}_{\mathrm{r}}(z) = -V(z,\Gamma)\tilde{\boldsymbol{y}}_{\mathrm{m}}(z) + S(z,\Gamma)\boldsymbol{d}_y(z), \\ S(z,\Gamma) = S_{\mathrm{m}}(z,\Gamma_{\mathrm{m}}) + S_w(z,\Gamma), \\ V(z,\Gamma) = I - S(z,\Gamma) = V_{\mathrm{m}}(z,\Gamma_{\mathrm{m}}) - S_w(z,\Gamma), \\ S_w(z) = W_{\mathrm{c}}(z,\Gamma_{\mathrm{c}})N_w(z,\Gamma_{\mathrm{m}})S_{\mathrm{m}}(z,\Gamma_{\mathrm{m}}), \end{cases} \tag{50}$$

where the pair $\{S, V\}$ is referred to as the *overall sensitivity* and *overall CS* as they account for the closed-loop plant, S_w is referred to as the *causality correction* and the expression of the factors can be found in [11]. The name *causality correction* indicates that S_w cannot be zeroed, $S_w \neq 0$, since the estimated noise $G\,\widehat{\boldsymbol{w}}\,(i)$ with $G = [G_{\mathrm{c}} \;\; QG_{\mathrm{d}}]$, cannot be canceled by the control law (49) because of causality. In fact, under white noise assumption, the noise one-step prediction is zero, i.e., $G\hat{\boldsymbol{w}}(i) = 0$, and the subtraction of a term proportional to $\widehat{\boldsymbol{w}}\,(i-1)$ in (49) just increases the tracking error covariance. Since in practice, due to inaccurate rejection, $G\hat{\boldsymbol{w}}(i)$ may include residual correlated components, they may be further attenuated by adding to (49) a stable dynamic feedback directly driven by $(\boldsymbol{y} - \hat{\boldsymbol{y}})(i)$ [20]. The term plays a role similar to Youla parameterization [21]. Let us observe that, at first sight, the CS $V_{\mathrm{c}}(z)$, which played a role in Section 2.3, does not appear in the last row of (50). Actually, we can prove that $V_{\mathrm{c}}(z) = W_{\mathrm{c0}}^{-1}W_{\mathrm{c}}(z)$, and being $V_{\mathrm{c}}(0) = I$ (low-pass filter), the frequency BW f_{c} of V_{c} can be defined.

In [11], S_w has been proved to be a band-pass transfer matrix, which makes the bandwidths $\{f_{\mathrm{s}}, f_{\mathrm{v}}\}$ of $\{S, V\}$ narrower than the BWs $\{f_{\mathrm{ms}}, f_{\mathrm{mv}}\}$ of $\{S_{\mathrm{m}}, V_{\mathrm{m}}\}$. Fig. 7 (a), clearly shows the phenomenon. Narrowing the sensitivity BW is detrimental to the tracking error accuracy ("bad effect") since the unknown disturbance rejection is band-limited. Narrowing the CS BW may be of benefit ("good effect") as it makes the state predictor more effective in blocking the contribution of the neglected dynamics to the control law. Equation (50) and the role of S_w look an advancement of the theory in Section 2.3, and are reflected by the last part of the error-loop block-diagram of Fig. 6.

The design implications of the new error loop in Fig. 6 can be better appreciated by extracting, from $\tilde{\boldsymbol{y}}_{\mathrm{m}}$ in (43) and $\boldsymbol{d}_y$ in (44) (in practice from $\boldsymbol{h}$), the uncertain components which depend on $\boldsymbol{y}_{\mathrm{m}}$ and hence on the tracking error, and therefore are prone to destabilize the closed-loop plant. Following [11], we rewrite (50) as

$$\begin{aligned} &(I + V(z,\Gamma)\partial P - S(z,\Gamma)\partial H)\tilde{\boldsymbol{y}}_{\mathrm{r}}(z) \\ &= (-V(z,\Gamma)\partial P + S(z,\Gamma)\partial H)\boldsymbol{r}(z) \\ &\quad - V(z,\Gamma)\boldsymbol{w}_{\mathrm{m}}(z) + S(z,\Gamma)D_y(z)\boldsymbol{w}(z), \end{aligned} \tag{51}$$

where the argument z has been partly omitted, $D_y(z)$ transfers the noise vector $\boldsymbol{w}$ onto $\boldsymbol{y}$, and $\partial H(z)$ is computed by assuming that $\boldsymbol{h}(\boldsymbol{x}_{\mathrm{c}})$ is a sector-bounded nonlinearity.

Closed-loop stability can be ensured by fixing the worst-case elements $\partial P_{\mathrm{worst}}(z) = \partial P(z, \boldsymbol{p}_{\mathrm{worst}})$ and $\partial H_{\mathrm{worst}}(z) = \partial H(z, \boldsymbol{p}_{\mathrm{worst}})$ of the uncertainty sets, and by applying either the Nyquist criterion or the small-gain theorem to the loop function $V(z)\partial P_{\mathrm{worst}}(z) -$

$S(z)\partial H_{\text{worst}}(z)$. Small-gain theorem allows the argument uncertainty to be ignored.

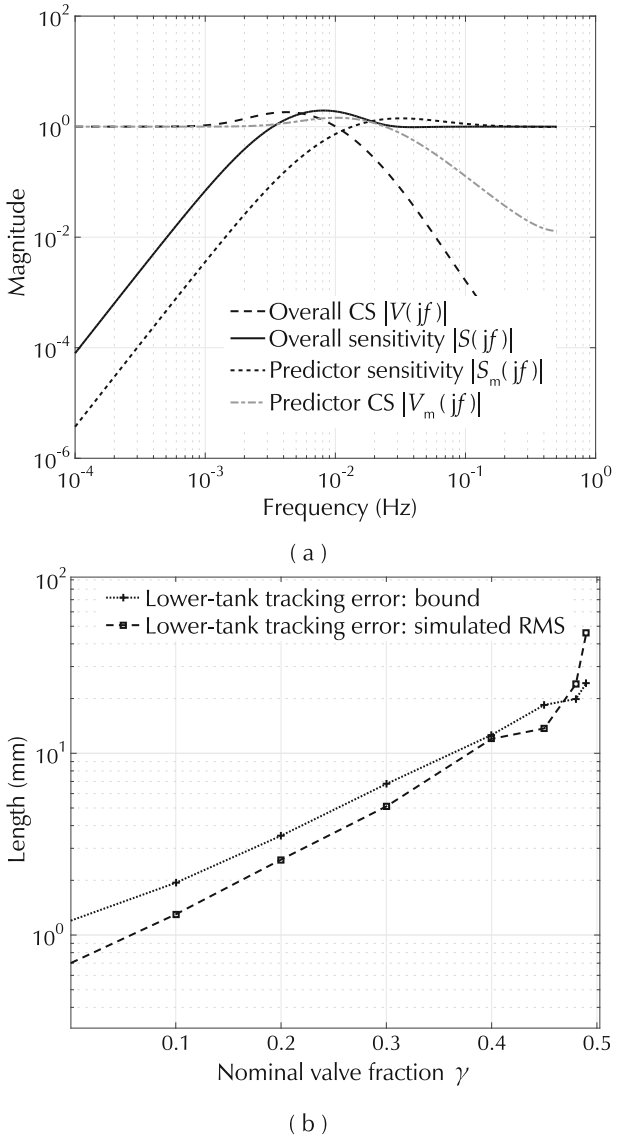

Fig. 7 (a) Case 1, state predictor and overall sensitivity, overall CS. (b) Tracking error RMS bound and simulated RMS.

If $\sigma_{\max}(\partial P_{\text{worst}}(\mathrm{j}f))$ and $\sigma_{\max}(\partial H_{\text{worst}}(\mathrm{j}f))$ dominate the high- and low-frequency bands of $0 \leqslant f < f_{\max}$, respectively, the small-gain inequality can be split into the pair of inequalities

$$\begin{cases} \eta_{\text{v}}^{-1}\|V(\mathrm{j}f,\Gamma)\partial P_{\text{worst}}(\mathrm{j}f)\|_\infty < 1, \\ \eta_{\text{s}}^{-1}\|S(\mathrm{j}f,\Gamma)\partial H_{\text{worst}}(\mathrm{j}f)\|_\infty < 1, \end{cases} \tag{52}$$

where the norms in (52) are defined by $\|E(\mathrm{j}f)\|_\infty = \max_{|f|\leqslant f_{\max}} \sigma_{\max}(E(\mathrm{j}f))$. The frequency domain separation in (52) can be further exploited by approximating $V(z)$ and $S(z)$ with their HF and LF asymptotes $V_\infty(z,\Gamma)$ and $S_0(z,\Gamma)$, respectively, as they are analytically related to the elements of Γ. Moreover, since the result of a pole placement which satisfies (52) is the frequency BW pair $\{f_{\text{s}}(\eta_{\text{s}}), f_{\text{v}}(\eta_{\text{v}})\}$, which is constrained by $f_{\text{s}}(\eta_{\text{s}}) < f_{\text{v}}(\eta_{\text{v}}) < f_{\max}$, failure of the latter inequality indicates that pole placement cannot ensure closed-loop stability versus the given uncertainty.

Given a feasible $\eta = \max\{\eta_{\text{s}}, \eta_{\text{v}}\} < 1$ and, for simplicity's sake, by assuming zero reference, i.e., $\boldsymbol{r} = 0$, (51) can be transformed into the pair of performance inequalities

$$\begin{cases} \dfrac{w_{\text{s}}}{1-\eta}\sigma_{\max}(V(\mathrm{j}f,\Gamma)S_w(f))\tilde{S}_{y,\max}^{-1}(f) \leqslant 1, \\ \dfrac{w_{\text{v}}}{1-\eta}\sigma_{\max}(S(\mathrm{j}f,\Gamma)S_{\text{d}}(f))\tilde{S}_{y,\max}^{-1}(f) \leqslant 1, \end{cases} \tag{53}$$

where $w_{\text{s}}^{-2} + w_{\text{v}}^{-2} = 1$, the frequency domain has been separated, $\{S_w, S_{\text{d}}\}$ denotes the spectral density bounds of $\boldsymbol{w}_{\text{m}}$ and $\boldsymbol{d}_y$, and $\tilde{S}_{y,\max}$ is the spectral bound of the output tracking error which is allocated to the pair of inequalities in (52) through the weight pair $\{\boldsymbol{w}_{\text{s}}, \boldsymbol{w}_{\text{v}}\}$. Stability and performance inequalities in (52) and (53) can be combined into a single functional to be minimized below unity. Moreover, performance inequalities can be converted into variance inequalities, which are equivalent to the weighted norm in (20).

The above inequalities are expressed in terms of $\{S(\Gamma), V(\Gamma)\}$, but which is the interplay with the SP pair $\{S_{\text{m}}(\Gamma_{\text{m}}), V_{\text{m}}(\Gamma_{\text{m}})\}$ of the first design step? Let $\{f_{\text{ms}}, f_{\text{mv}}\}$ be the frequency BW pair of the state predictor (SP). Two pole placement strategies have been pointed out in [11].

1) The *standard design* guarantees that the SP sensitivity is not degraded by S_w, which amounts to satisfy the frequency inequality

$$f_{\text{ms}} \cong f_{\text{s}} < f_{\text{mv}} < f_{\text{c}} < f_{\max}, \tag{54}$$

where f_{c} is the frequency BW of V_{c}. The inequality implies and is implied by $\|S_w\|_\infty < 1$, and in turn implies that the norm of the measured tracking error $|\boldsymbol{r} - \hat{\boldsymbol{y}}|$ tends to be a numerical zero, smaller than the output quantization, a condition that can be in-field verified.

2) The *nonstandard design* aims to $f_{\text{c}} < f_{\text{mv}}$ and implies $f_{\text{s}} < f_{\text{ms}}$, with the consequence that the SP sensitivity is degraded as in Fig. 7 (a). The design becomes mandatory to account for command saturation and for avoiding saturation instability. The case study of Section 4 will adopt this strategy, since "crude" command saturation is allowed between two successive set points.

4 Case study

The EMC design steps in Section 3 are now applied to a well-known multivariate control problem.

4.1 From tank dynamics to the design model

Consider the four-tank control problem in [13]; the layout is sketched in Fig. 8.

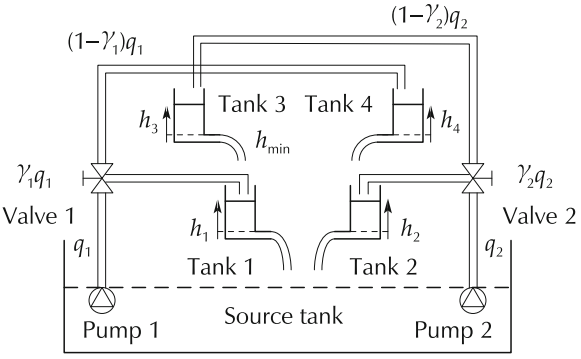

Fig. 8 Sketch of the four-tank layout.

Two pairs of cascaded tanks $\{k = 1,3\}$ and $\{k = 2,4\}$ are fed by two pumps denoted by the subscript $\{j = 1,2\}$. The pair of lower tanks $\{k = 1,2\}$ discharges into the common source tank and are fed by one of the upper tanks and by one of the pumps with the rule: $\{j = 1, k = 3\} \to k = 1$ and $\{j = 2, k = 4\} \to k = 2$. The pair of upper tanks $\{k = 3,4\}$ is just fed by the pumps with the reverse rule of the lower tanks, i.e., $j = 1 \to k = 4$ and $j = 2 \to k = 3$. The pump flows are distributed to tanks by regulating the valves 1 and 2 to the fractions $0 \leqslant \gamma_1 \leqslant 1$ and $0 \leqslant \gamma_2 \leqslant 1$. The fractions are collected in the vector $\boldsymbol{\gamma} = [\gamma_1, \gamma_2]$ (inline vector notation). The kth tank level x_k is bounded by $0 \leqslant x_{k,\min} \leqslant x_k \leqslant x_{k,\max}$ and is an entry of the vector $0 \leqslant \boldsymbol{x} \leqslant \boldsymbol{x}_{\max}$. The level square root $\sqrt{x_k}$ defines the tank discharge rate $p_k = S_k^{-1}\alpha_k\sqrt{2\mathrm{g}x_k} = \beta_k\sqrt{x_k}$, where S_k is the horizontal section area, α_k is the discharge constant in m^2 and g is the local gravity. The pump flow rate $0 \leqslant q_k{=}\phi_k/S_k\,(\mathrm{m}\cdot\mathrm{s}^{-1}) \leqslant q_{k,\max}$ is collected in the vector $\boldsymbol{q}$ and depends on the pump command vector $[\phi_1, \phi_2]\,(\mathrm{m}^3\cdot\mathrm{s}^{-1})$.

The nonlinear fourth-order state equation (see [22]) is written, without initial conditions, as

$$\begin{cases} \dot{\boldsymbol{x}}(t) = A\sqrt{\boldsymbol{x}} + B\boldsymbol{q}(t-\tau_u) + \boldsymbol{q}_{\mathrm{d}}(t), \\ \boldsymbol{y}(t) = C\boldsymbol{x}(t-\tau_y) + \tilde{\boldsymbol{y}}_{\mathrm{m}}(t), \end{cases} \tag{55}$$

where $0 \leqslant \boldsymbol{x} \leqslant \boldsymbol{x}_{\max}$, $0 \leqslant \boldsymbol{q}(t) \leqslant \boldsymbol{q}_{\max}$, τ_u is a transport delay, τ_y is the level sensor delay, $\boldsymbol{y}$ is the tank level measurement corrupted by $\tilde{\boldsymbol{y}}_{\mathrm{m}}$, $\boldsymbol{q}_{\mathrm{d}}$ collects the flow perturbations due to leakage and model inaccuracy, and the following notations apply:

$$\begin{cases} \boldsymbol{x} = \begin{bmatrix} \boldsymbol{x}_{12} \\ \boldsymbol{x}_{34} \end{bmatrix}, \quad \boldsymbol{x}_{12} = \begin{bmatrix} x_1 \\ x_2 \end{bmatrix}, \quad \boldsymbol{x}_{34} = \begin{bmatrix} x_3 \\ x_4 \end{bmatrix}, \\ \sqrt{\boldsymbol{x}} = [\,\sqrt{x_1}\ \cdots\ \sqrt{x_4}\,], \quad C = \mathrm{diag}\{c_1, c_2, c_3, c_4\}, \\ A = \left[\begin{array}{cc|cc} -\beta_1 & 0 & \beta_3 & 0 \\ 0 & -\beta_2 & 0 & \beta_4 \\ \hline 0 & 0 & -\beta_3 & 0 \\ 0 & 0 & 0 & -\beta_4 \end{array}\right] \\ B = \left[\begin{array}{cc} \gamma_1 & 0 \\ 0 & \gamma_2 \\ \hline 0 & (1-\gamma_2)\dfrac{S_2}{S_3} \\ (1-\gamma_1)\dfrac{S_1}{S_4} & 0 \end{array}\right], \end{cases} \tag{56}$$

where B can also be written as $B = [B_{12}\ \ B_{34}]$. In (56), $\boldsymbol{q}_{\max}$ is the pump maximum flow and $c_k = 1 + s_k$, $s_k \ll 1$ being the scale factor error. As soon as $\boldsymbol{x} \to 0$, the measurement error $\tilde{\boldsymbol{y}}_{\mathrm{m}}$ becomes biased by the least measured level denoted by $\boldsymbol{x}_{\min} > 0$. The limit will be employed by the control unit to bound $\boldsymbol{x}$ from below, when necessary.

The control goal is to force the lower-tank levels in $\boldsymbol{x}_{12}$ to track the reference $\boldsymbol{r}_{12} = [r_1, r_2]$, where, as in [22], the reference profile is a sequence of set points, which are equilibrium points of (55). Given the equilibrium vector $\underline{\boldsymbol{x}}_{12}$ satisfying the limits in (56), the command and upper tank equilibrium values $\underline{\boldsymbol{q}} = [\underline{q}_1, \underline{q}_2]$ and $\underline{\boldsymbol{x}}_{34}$ are given by

$$\begin{cases} \begin{bmatrix} \beta_1\sqrt{\underline{x}_1} \\ \beta_2\sqrt{\underline{x}_2} \end{bmatrix} = G\underline{\boldsymbol{q}}, \quad \begin{bmatrix} \beta_3\sqrt{\underline{x}_3} \\ \beta_4\sqrt{\underline{x}_4} \end{bmatrix} = B_{34}\underline{\boldsymbol{q}}, \\ G = \begin{bmatrix} \gamma_1 & (1-\gamma_2)S_2/S_3 \\ (1-\gamma_1)S_1/S_4 & \gamma_2 \end{bmatrix}, \\ \det G = \gamma_1\gamma_2\left(1 - \sigma\dfrac{(1-\gamma_1)(1-\gamma_2)}{\gamma_1\gamma_2}\right), \ \sigma = \dfrac{S_1S_2}{S_3S_4} > 0. \end{cases} \tag{57}$$

The zero determinant $\det G = 0$ distinguishes two regulation problems.

1) *Direct lower tank regulation* for $\det G > 0$. The corresponding inequality $(1/\gamma_1 - 1)(1/\gamma_2 - 1) < 1/\sigma$ implies the valve fraction direction $\boldsymbol{\gamma} \to [1,1]$ and the convergence to $\det G = 1$. Under this condition (see Fig. 8), the lower tanks can be directly and independently regulated to the set point $\underline{\boldsymbol{x}}_{12}$, which must satisfy the pump flow

and upper tank limits. The lower tank dynamics is just first order. The upper tank dynamics, under the lower-tank regulation, plays the role of a zero dynamics [14], which is locally asymptotically stable. The corresponding discharge flow is treated as a disturbance.

2) *Indirect lower tank regulation* for $\det G < 0$. The corresponding inequality $(1/\gamma_1 - 1)(1/\gamma_2 - 1) > 1/\sigma$ implies the valve fraction direction $\boldsymbol{\gamma} \to [0, 0]$, and the convergence to $\det G = -\sigma$. Under this condition (see Fig. 8), the lower tanks must be regulated through the upper tanks and the input-output relative degree becomes two. In fact, for $\det G = -\sigma$, as proven in [22] and [23], the upper tank dynamics, under direct lower tank regulation, becomes a locally unstable zero dynamics [14] and the upper tank levels tend to saturate. Unlike in [23], where a combination of the lower and tank levels was regulated ([22] showed that a mixed regulation cannot regulate the lower tanks in the presence of unknown disturbances), Section 4.2 and the following will show that the indirect regulation cannot just be addressed by converting (55) into the normal form of the feedback linearization [14], since the resulting normal form happens to be driven by the derivative of the pump flow, and the relevant extended dynamics [14] is nonlinear, uncertain and affected by a non-collocated disturbance. Moreover, since any disturbance flow affecting the lower tanks will be accommodated by the varying level and discharge rate of the upper tanks, level set-points must be carefully selected.

The indirect regulation has been approached in [24] by the sliding model control in the region $0.1 \leqslant \gamma_1, \gamma_2 \leqslant 0.2$. Here, the first step is to derive a CT design model via feedback linearization and extended dynamics (Section 4.2). A LTI design model is the basis for building the stabilizing ideal control law in Section 4.3. The same model is the source of the DT embedded model (57) in Section 4.4. In the same Section, the model is stabilized by a dynamic noise estimator of the same kind as in equation (45) and the ideal control law is converted into its real form. Section 4.5 is devoted to the pole placement in the presence of causal uncertainty (random flows), parametric uncertainty and neglected dynamics. The design inequalities of Section 3.2 will be employed. A nonstandard pole placement is adopted to cope with 'crude' pump-flow saturation during set-point switching. Section 4.6 will illustrate and discuss simulated results in the fraction region $0 \leqslant \gamma_1, \gamma_2 < 0.5$, to check the previous design in the presence of uncertainty.

4.2 The design model

In view of the indirect regulation, we transform the fourth-order equation (55) into a non-minimum-phase sixth-order equation with zero eigenvalues and one positive transmission zero. Let us define the controllable state $\boldsymbol{x}_\mathrm{c}$ through a smooth transformation $\boldsymbol{f}(\boldsymbol{x}), \boldsymbol{x} > 0$, and the inclusion of the pump flow rate $\boldsymbol{q}$:

$$\begin{cases} \boldsymbol{x}_\mathrm{c} = \begin{bmatrix} \boldsymbol{x}_{12} \\ \boldsymbol{v}_{12} \\ \boldsymbol{q} \end{bmatrix} = \begin{bmatrix} \boldsymbol{x}_{12} \\ \boldsymbol{f}(\boldsymbol{x}) \\ 0 \end{bmatrix} + \begin{bmatrix} 0 \\ B_{12} \\ I \end{bmatrix} \boldsymbol{q}, \\ \boldsymbol{v}_{12} = \begin{bmatrix} v_1 \\ v_2 \end{bmatrix} = \dot{\boldsymbol{x}}_{12}, \\ f(\boldsymbol{x}) = \begin{bmatrix} -\beta_1 \sqrt{x_1} + \beta_3 \sqrt{x_3} \\ -\beta_2 \sqrt{x_2} + \beta_4 \sqrt{x_4} \end{bmatrix}, \end{cases} \tag{58}$$

where $\sqrt{x_{k+2}(\boldsymbol{x}_\mathrm{c})} = (v_k + \beta_k \sqrt{x_k})/\beta_{k+2}$. The derivative of $\boldsymbol{x}_\mathrm{c}$ and the new command $\boldsymbol{u} = \dot{\boldsymbol{q}}$ provide the following state equation:

$$\begin{cases} \dot{\boldsymbol{x}}_\mathrm{c}(t) = \begin{bmatrix} 0 & I & 0 \\ 0 & 0 & G_{34}(\boldsymbol{x}_\mathrm{c}) \\ 0 & 0 & 0 \end{bmatrix} \boldsymbol{x}_\mathrm{c}(t) + \begin{bmatrix} 0 \\ B_{12} \\ I \end{bmatrix} \boldsymbol{u}(t - \tau_u) \\ \qquad\qquad + \begin{bmatrix} 0 \\ \boldsymbol{d}(t) + \boldsymbol{h}(\cdot) \\ 0 \end{bmatrix}, \\ \boldsymbol{y}(t) = [C_{12}\ 0\ \ 0] \boldsymbol{x}_\mathrm{c}(t - \tau_y) + \tilde{\boldsymbol{y}}_\mathrm{m}(t), \end{cases} \tag{59}$$

where initial conditions have been omitted, $\boldsymbol{d} = [d_1, d_2]$ is the unknown disturbance, $\boldsymbol{h}(\cdot)$ is a cross-coupling term, and the following notations apply:

$$\begin{cases} G_{34}(\boldsymbol{x}_\mathrm{c}) = P_{34}(\boldsymbol{x}_\mathrm{c}) B_{34}, \\ P_{34}(\boldsymbol{x}_\mathrm{c}) = \begin{bmatrix} p_3(\boldsymbol{x}_\mathrm{c}) > 0 & 0 \\ 0 & p_4(\boldsymbol{x}_\mathrm{c}) > 0 \end{bmatrix}, \\ P_{12}(\boldsymbol{x}_\mathrm{c}) = \begin{bmatrix} p_1(\boldsymbol{x}_\mathrm{c}) > 0 & 0 \\ 0 & p_2(\boldsymbol{x}_\mathrm{c}) > 0 \end{bmatrix}, \\ \boldsymbol{h}(\cdot) = -P_{12}(\boldsymbol{x}_\mathrm{c}) v_{12} + \begin{bmatrix} \dfrac{-\beta_3^2}{2} \\ \dfrac{-\beta_4^2}{2} \end{bmatrix}, \\ p_k(\boldsymbol{x}_\mathrm{c}) = \dfrac{\beta_k}{2\sqrt{x_k(\boldsymbol{x}_\mathrm{c})}}\ (\mathrm{rad} \cdot \mathrm{s}^{-1}), \quad k = 1, 2, 3, 4, \\ C_{12} = \mathrm{diag}\{c_1, c_2\}. \end{cases} \tag{60}$$

The pair of variable transmission zeros holds

$$z_{1,2} = \pm\sqrt{\frac{(1-\gamma_1)(1-\gamma_2)S_1S_2}{\gamma_1\gamma_2S_3S_4}p_3p_4}. \tag{61}$$

The state-dependent matrix $G_{34}(\boldsymbol{x}_c)$ can be confined into the command matrix, but the state-feedback design does not change, since the relative degree does not change from two to three and a normal form cannot be obtained.

Fig. 9 shows the block diagram of (59). Delays are represented by blocks with an inscribed D. A double-border box denotes a nonlinear function. The variable gain p_k is denoted with an arrowed circle. Vertical arrows denote initial conditions. The parameters $b_k, k = 1,\ldots,4$, are the nonzero entries of the matrix B in (56), the subscript k being the row index of B.

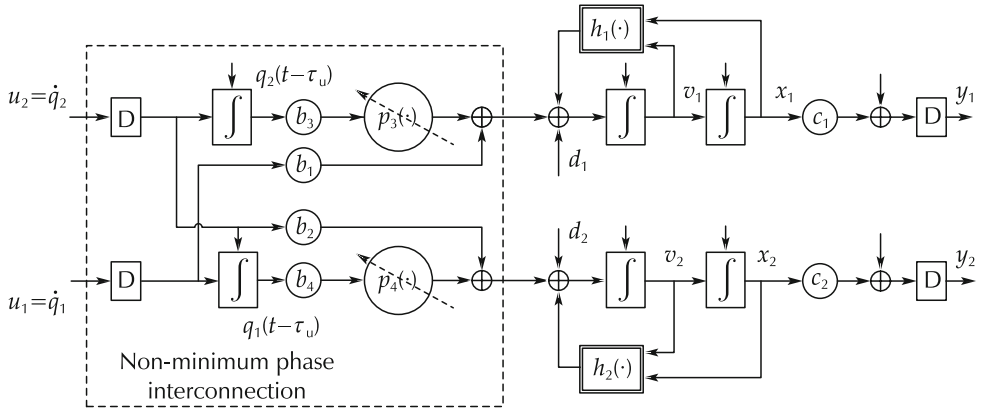

Fig. 9 Block diagram of the design model.

4.3 Ideal control law

Let us neglect the command delay τ_u (to be part of neglected dynamics), and include $\boldsymbol{h}(\cdot)$ (assumed to be unknown) into $\boldsymbol{d}$. Let the tracking error of the lower tanks be written as $\tilde{\boldsymbol{x}}_{12r} = \boldsymbol{x}_{12} - \boldsymbol{x}_{12r}$, where $\boldsymbol{x}_{12r} = \underline{\boldsymbol{x}}_{12}$ (the set point) is a sequence of equilibrium points in (57) satisfying tank and pump bounds. Similarly, we define the level rate error $\tilde{\boldsymbol{v}}_{12r} = \boldsymbol{v}_{12}$ and the flow rate error $\tilde{\boldsymbol{q}}_r = \boldsymbol{q} - \boldsymbol{q}_r + Q(\boldsymbol{x})\boldsymbol{d}$, where $\boldsymbol{q}_r = \underline{\boldsymbol{q}}$ has been defined in (57), and Q testifies that $\boldsymbol{d}$ is not collocated. The ideal stabilizing control law of (59) is given by

$$\boldsymbol{u}(t) = -(K_x\tilde{\boldsymbol{x}}_{12r} + K_v\tilde{\boldsymbol{v}}_{12r} + K_q\tilde{\boldsymbol{q}}_r), \tag{62}$$

where the identity $K_x = K_x(\boldsymbol{x}_c)$ applies to the three gain matrices, which depend on $\boldsymbol{x}_c$ through $G_{34}(\boldsymbol{x}_c)$. Because of the bound $|\boldsymbol{x}_c| \leqslant \boldsymbol{x}_{c,max}$, which derives from the bounded $\boldsymbol{x}$ and $\boldsymbol{q}$ in (56), $G_{34}(\boldsymbol{x}_c) > 0$ is bounded from below and from above and the feedback gains in (62) can be designed by assuming that the nominal matrices $\underline{G}_{34}(\boldsymbol{x}_r) > 0$ and $\underline{B}_{12} \geqslant 0$ are symmetric and constant during a set-point interval of the reference profile $\boldsymbol{x}_r(t) = [\boldsymbol{x}_{12r}, \boldsymbol{x}_{34r}]$. The matrix discrepancy $G_{34}(\boldsymbol{x}_c) - \underline{G}_{34}(\boldsymbol{x}_r)$ holds:

$$G_{34}(\boldsymbol{x}_c) - \underline{G}_{34}(\boldsymbol{x}_r) = \Delta G_{34}(\boldsymbol{x}_c) + \delta P_{34}(\tilde{\boldsymbol{x}}_r)\underline{B}_{34} + o(|\tilde{\boldsymbol{x}}_r|^2),$$

$$\begin{aligned}
&\Delta G_{34}(\boldsymbol{x}_c) = \Delta P_{34}(\cdot)\underline{B}_{34} + P_{34}(\cdot)\Delta B_{34},\\
&\Delta P_{34}(\boldsymbol{x}_c) = \frac{1}{2}\mathrm{diag}\{\frac{\Delta\beta_k}{\sqrt{x_k(\boldsymbol{x}_c)}},\ k = 3,4\},\\
&\delta P_{34}(\tilde{\boldsymbol{x}}_r) = -\frac{1}{4}\mathrm{diag}\{\frac{\underline{\beta}_k\tilde{\boldsymbol{x}}_{kr}/\sqrt{x_{kr}}}{x_{kr}},\ k = 3,4\},
\end{aligned} \tag{63}$$

where $(\cdot)$ means $(\boldsymbol{x}_c)$, $\underline{\beta}_{k+2}\tilde{x}_{k+2}/\sqrt{x_{k+2,r}} = 2(\tilde{v}_{kr} + \underline{p}_k(x_{kr})\times\tilde{x}_{kr})$, $k = 1,2$, $\Delta B_{34} = B_{34} - \underline{B}_{34}$, and all the matrices are bounded. Under the previous assumptions, the attribute "ideal" means that the tracking errors in (62) are perfectly known. The symmetric and constant feedback matrices in $\{K_x, K_v, K_q\}$ that stabilize the closed-loop state matrix A_c are as follows:

$$\begin{cases}
A_c = -\begin{bmatrix} 0 & I & 0 \\ \underline{B}_{12}K_x & \underline{B}_{12}K_v & B_{12}K_q - \underline{G}_{34} \\ K_x & K_v & K_q \end{bmatrix},\\
\underline{B}_{12} = \begin{bmatrix} b & 0 \\ 0 & b \end{bmatrix} \geqslant 0,\ \ \underline{G}_{34} = \begin{bmatrix} 0 & g \\ g & 0 \end{bmatrix} \geqslant 0,\\
K_x = \begin{bmatrix} k_{1x} & k_{2x} \\ k_{2x} & k_{1x} \end{bmatrix},\ \ K_v = \begin{bmatrix} k_{1v} & k_{2v} \\ k_{2v} & k_{1v} \end{bmatrix},\ \ K_q = \begin{bmatrix} k_{1q} & k_{2q} \\ k_{2q} & k_{1q} \end{bmatrix}.
\end{cases} \tag{64}$$

Because of the aforementioned symmetry, the characteristic polynomial $\Pi(A_c, \lambda)$ can be factored into a pair of third-order polynomials, whose coefficients are related to the sub-matrix entries in (64). Given a Hurwitz spectrum $\Lambda_c = \Lambda(A_c)$ and the coefficients in

$$\Pi(A_c, \lambda) = \prod_{i=1}^{2}(\lambda^3 + c_{2i}\lambda^2 + c_{1i}\lambda + c_{0i}), \tag{65}$$

the gains in (64) are found by solving an algebraic equation, which admits a unique solution for $b = \underline{\gamma}_1 = \underline{\gamma}_2 < 1$ in the matrix $\underline{B}_{12}$. $Q(\boldsymbol{x}_r) = \underline{G}_{34}^{-1}(\boldsymbol{x}_r)$ can be found from the Davison-Francis equation (48), if applied to the embedded model of Section 4.4.

4.4 Embedded model and real control law

The next step amounts to convert (59) into a DT embedded model like that in equation (42). The model must include the disturbance dynamics and must provide the one-step prediction of the command before $t_{i+1} = (i+1)T$. The real control law generates the plant command as the digitized pump flow $\boldsymbol{n}_q$ and the flow rate derivative in (62) as a function of the measured tracking errors as follows:

$$\begin{cases} \boldsymbol{u}(i) = -(K_x \boldsymbol{e}_{xr} + K_v \boldsymbol{e}_{vr} + K_q \boldsymbol{e}_{qr}), \\ \boldsymbol{e}_{xr} = \hat{\boldsymbol{x}}_{12} - \boldsymbol{x}_{12r}, \;\; \boldsymbol{e}_{vr} = \hat{\boldsymbol{v}}_{12} \; (\mathrm{m \cdot s^{-1}}), \\ \boldsymbol{e}_{qr} = \hat{\boldsymbol{q}} - \boldsymbol{q}_r + Q(\boldsymbol{x}_r)\hat{\boldsymbol{x}}_d \; (\mathrm{m \cdot s^{-1}}), \\ \boldsymbol{n}_q(i+1) = \mathrm{int}(R_q^{-1}\hat{\boldsymbol{q}}), \;\; 0 \leqslant \boldsymbol{n}_q < \boldsymbol{N}_q, \end{cases} \tag{66}$$

where the time i has been partly omitted, the last row expresses command digitization and saturation, $\boldsymbol{n}_q(i)$ and $\boldsymbol{N}_q$ are integer vectors and R_q holds:

$$R_q = \mathrm{diag}\{\rho_{q1}, \rho_{q2}\}, \;\; \rho_{qk} = q_{k,\max}/N_{qk}, \tag{67}$$

where $k = 1, 2$.

The embedded model aims to one-step predicting the controllable state $\{\hat{\boldsymbol{x}}_{12}, \hat{\boldsymbol{v}}_{12}, \hat{\boldsymbol{q}}\}$ and the unknown disturbance $\hat{\boldsymbol{x}}_d(i)$ (in acceleration units). The possible improvement of the one-step prediction in (66) by the current measurement $\boldsymbol{y}(i)$ is not considered. The pair of decoupled fourth-order equations, in the form of (42), is as follows:

$$\begin{bmatrix} \hat{\boldsymbol{x}}_{12} \\ \hat{\boldsymbol{v}}_{12} \\ \hat{\boldsymbol{q}} \\ \hat{\boldsymbol{x}}_d \end{bmatrix}(i+1) = \begin{bmatrix} I & IT & 0 & 0 \\ 0 & I & \underline{G}_{34} & IT \\ 0 & 0 & I & 0 \\ 0 & 0 & 0 & I \end{bmatrix} \begin{bmatrix} \hat{\boldsymbol{x}}_{12} \\ \hat{\boldsymbol{v}}_{12} \\ \hat{\boldsymbol{q}} \\ \hat{\boldsymbol{x}}_d \end{bmatrix} + \begin{bmatrix} 0 \\ \underline{B}_{12}T \\ IT \\ 0 \end{bmatrix} \boldsymbol{u} + \begin{bmatrix} 0 \\ \widehat{\boldsymbol{w}}_c \\ 0 \\ \widehat{\boldsymbol{w}}_d \end{bmatrix},$$

$$\hat{\boldsymbol{y}}(i) = [I \;\; 0 \;\; 0 \;\; 0] \begin{bmatrix} \hat{\boldsymbol{x}}_{12} \\ \hat{\boldsymbol{v}}_{12} \\ \hat{\boldsymbol{q}} \\ \hat{\boldsymbol{x}}_d \end{bmatrix}, \tag{68}$$

where time i has been partly omitted, the unknown disturbance is the sum of the noise $\widehat{\boldsymbol{w}}_c$ (including the command quantization error) and of the first-order random drift $\hat{\boldsymbol{x}}_d$ driven by the noise $\widehat{\boldsymbol{w}}_d$. In practice, the three equations of (59) are completed with that of $\hat{\boldsymbol{x}}_d$. Transport and sensor delays are confined into the neglected dynamics. Parametric errors come from the uncertainty of B_{12} and the uncertainty and time variability of G_{34}.

The matrix G_c of (42) that multiplies $\widehat{\boldsymbol{w}}_c$ is singular, since no component is driving the first and third rows of (68). The zero first row implies that a dynamic noise estimator H must be adopted, as in [11] and in equation (45) in order to stabilize the embedded model. In this case, only four diagonal matrices $\{A_e, L_c, N_c, N_d\}$ are necessary and sufficient to stabilize the pair of fourth-order state predictors, which consists of (68), without the third row, and of (45) with $L_d = 0$. The one-to-one relation between the AS spectrum $\Lambda_m = \{\Lambda_{mk}, k = 1, 2\}$ with $\Lambda_{mk} = \{\lambda_{mkj}, j = 1, \ldots, 4\}$, $|\lambda_{mkj}| < 1$, and the eight gains of the diagonal feedback matrices $\{A_e, L_c, N_c, N_d\}$ is straightforward (see [11]).

4.5 Pole placement

The assignment of the complementary spectra Γ_c (control law) and Γ_m (SP), which possess a total of 7+7 eigenvalues, is driven by two objectives. The first one is *asymptotic stability* in the presence of uncertainty and pump flow saturation. The second is the *accuracy* of the lower tank level around the required set points in the presence of random flows, measurement errors and parametric uncertainty. We assume that the nominal valve fractions are uniform and equal, i.e., $\underline{\gamma}_k = \underline{\gamma} < 0.5$, $k = 1, 2$.

4.5.1 Stability

We do not adopt a reference generator that minimizes the tracking error during set-point switching. This implies "crude" saturation of pump flows and instability because of the relative degree > 1. According to EMC design [11], command saturation can be managed by adopting the non-standard design of Section 3.2 (an alternative solution is to shape the feedback gains as satu-

rating functions). In essence, we adopt $f_{\rm c}(\Gamma_{\rm c}) < f_{\rm mv}(\Gamma_{\rm m})$ where $f_{\rm c}$ refers to $V_{\rm c}(\Gamma_{\rm c})$ and $f_{\rm mv}$ to $V_{\rm m}(\Gamma_{\rm m})$. In terms of the real complementary eigenvalues $\gamma_{{\rm c}j}(\underline{\gamma}) \in \Gamma_{\rm c}$, $j = 1,\ldots,6$ and $\gamma_{{\rm m}j} \in \Gamma_{\rm m}$, $j = 1,\ldots,8$, we impose the inequalities

$$\begin{aligned} 0 < \gamma_{\rm c,max} &= \max_j\{\gamma_{{\rm c}j}\} \\ &< \max_j\{\gamma_{{\rm m}j}\} = \gamma_{\rm m,max} \leqslant 1, \end{aligned} \tag{69}$$

where $\gamma_{{\rm c}j} = \gamma_{{\rm c}j}(\underline{\gamma})$ depends on the fraction $\underline{\gamma}$, as it enters $\underline{G}_{34}$ and $\underline{B}_{12}$ in (68). By means of the circle criterion [14], the following upper bound has been found for the simulated case study:

$$\gamma_{\rm c,max} \leqslant \gamma_{\rm m,max} - \beta\underline{\gamma}^{\varepsilon},\ \gamma_{\rm m,max} = 0.2,\ \beta = 0.25,\ \varepsilon = 0.7. \tag{70}$$

Following [11], the eigenvalues are spread with the following rules

$$\begin{cases} \gamma_{{\rm c}j} = \gamma_{\rm c,max} 2^{-\alpha_{\rm c}(j-1)},\ j = 1,2,3, \\ \gamma = \gamma_{\rm m,max} 2^{-\alpha_{\rm m}(j-1)},\ j = 1,\ldots,4, \end{cases} \tag{71}$$

where $\{\alpha_{\rm c} \geqslant 0, \alpha_{\rm m} \geqslant 0\}$ is a second pair of tunable parameters.

Given (70), $\{\alpha_{\rm c}, \alpha_{\rm m}\}$ have been tuned for guaranteeing closed-loop stability versus neglected dynamics due to delays and the parametric uncertainty $\Delta G_{34}(\boldsymbol{x}_{\rm c}) + \delta P_{34}(\tilde{\boldsymbol{x}}_{\rm r})\underline{B}_{34}$ in (63). To be simple, we only focus on the fractional error ∂P in (51), by including $\Delta G_{34}(\boldsymbol{x}_{\rm c})$ in ∂P. The effect of $\delta P_{34}(\tilde{\boldsymbol{x}}_{\rm r})\underline{B}_{34}$ as a component of ∂H will not be studied. The design inequality to be adopted is just the first row in (52).

In order to build up ∂P, we treat $G_{34}(\boldsymbol{x}_{\rm c})$ and $P_{12}(\boldsymbol{x}_{\rm c})$ as perturbed constant matrices, which allows us to write $P(s)$ appearing in the transfer relation $\boldsymbol{x}_{12}(s) = P(s)\boldsymbol{q}(s)$ (design model) as follows:

$$\begin{aligned} P(s) = {\rm e}^{-s\tau}s^{-1}(sI + P_{12})^{-1}(&\underline{G}_{34}(x_{\rm r}) \\ &+ \Delta G_{34} + s(\underline{B}_{12} + \Delta B_{12})), \end{aligned} \tag{72}$$

where $\tau = \tau_q + \tau_y \leqslant 2$ s is the unknown total delay and P_{12} is a bounded unknown. The zero-order interpolated transfer matrix in $\hat{\boldsymbol{x}}_{12}(s) = M(s)\boldsymbol{q}(s)$ (embedded model) holds

$$\begin{aligned} M(s) &= \frac{{\rm e}^{-sT}}{s(z-1)}(T\underline{G}_{34}(\boldsymbol{x}_{\rm r}) + (z-1)\underline{B}_{12}) \\ &\cong s^{-2}(\underline{G}_{34}(\boldsymbol{x}_{\rm r}) + \frac{s\underline{B}_{12}}{T}), \end{aligned} \tag{73}$$

where $z = \exp(sT)$ with $s = {\rm j}2\pi f$, and the second-row approximation applies for $f < \pi/T$.

The open-loop fractional error $\partial P(s) = P(s)M^{-1}(s) - I$ turns out to be unstable, since one of the transmission zeros of $M(s)$ is real positive as pointed out by (61). However, the closed-loop $V(s)\partial P(s)$ is internally stable, since the transmission zeros of $V(s)$ include those of $M(s)$, and thus cancel the poles of $M^{-1}(s)$. We have to guarantee stability in the presence of the worst-case $\partial P_{\rm worst}(s)$, which corresponds either to $G_{34,\max} = G_{34}(\boldsymbol{x}_{34r,\min})$ or to $G_{34,\min} = G_{34}(\boldsymbol{x}_{34r,\max})$ depending on $\underline{G}_{34}(\boldsymbol{x}_{\rm r})$. The resulting pair $\{\alpha_{\rm c}, \alpha_{\rm m}\}$ is reported in Table 1.

Table 1 Control unit parameters and simulation results.

No	Parameter	Symbol	Unit	Value	Comment
		Control unit			
1	Time unit	T	s	1	
2	SP eigenvalues	$\gamma_{\rm m,max}, \alpha_{\rm m}$		0.2, 1.0	Both cases
3	Sensitivity BW	$f_{\rm ms}$	mHz	7	$S_{\rm m}$
4	CL, Case 1	$\gamma_{\rm c,max}, \alpha_{\rm c}$		0.075, 1.2	$\gamma = 0.1$
5	Sensitivity BW	$f_{\rm s}$	mHz	3.3	S
6	CL, Case 2	$\gamma_{\rm c,max}, \alpha_{\rm c}$		0.029, 1.2	$\gamma = 0.45$
7	Sensitivity BW	$f_{\rm s}$	mHz	1.35	S
		Simulation results: True tracking error of the lower tanks (RMS)			
8	Case 1	$\tilde{\sigma}_{xk}, k = 1,2$	mm	1.3	$\gamma = 0.1$
9	Case 2	$\tilde{\sigma}_{xk}, k = 1,2$	mm	13.7	$\gamma = 0.45$

As a check, the Nyquist plot of $\det(I+\partial P_{\text{worst}}(j\omega))-1$ (the open-loop case) and of $\det(I+V(j\omega)\partial P_{\text{worst}}(j\omega))-1$ (the closed-loop case) are shown in Fig. 10, for $\underline{\gamma}=0.1$ (simulated Case 1, Fig. 10 (a)), for $\underline{\gamma}=0.45$ (simulated Case 2, Fig. 10 (b)) and for the pair $\{G_{34,\min}, G_{34,\max}\}$. Since $V(s)\partial P_{\text{worst}}(s)$ has no unstable poles, both Nyquist plots ensure closed-loop stability as they do not encircle the critical point $(-1,0)$.

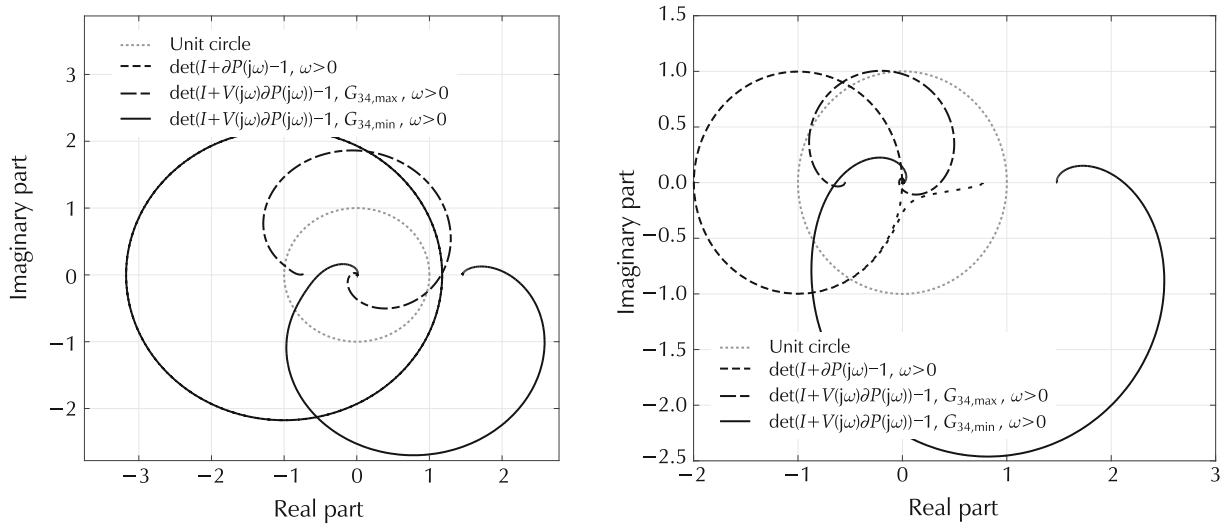

Fig. 10 Nyquist plot of the open loop and closed-loop fractional error for the pair $\{G_{34,\min}, G_{34,\max}\}$. The large closed curve corresponds to the open-loop case. (a) Case1. (b) Case 2.

4.5.2 Accuracy

"Crude" saturation suggests that accuracy requirement only concerns steady state level fluctuations and the transient time duration τ_j since the switching time t_{rj}. The accuracy indicator is the a posteriori RMS $\|\tilde{x}_k = x_k - x_{kr}\|$ of the tracking error $\tilde{x}_k$, which is defined by

$$\|\tilde{x}_k\| = \sqrt{\frac{\sum_{j=0}^{n_r}\sum_{i=0}^{N_j-1}\tilde{x}_k^2(i+\frac{t_{rj}}{T}+\frac{\tau_j}{T})}{\sum_{j=0}^{n_r}N_j}}, \tag{74}$$

for $N_jT \leqslant t_{r,j+1}-(t_{rj}+\tau_j)$. Given the pole placement in (69) and (70), accuracy can only be predicted from the inequalities in (53). The first one is concerned with the measurement noise, whose contribution can be proved, in the present simulated case, to be less significant than the random flow q_d in (55). Thus, we restrict the analysis to the second inequality, where $S_d(f)$ $(\text{m}\cdot(\sqrt{\text{Hz}})^{-1})$ is the spectral bound, in length units, of the random flow components q_{d1}, $k=1,2$ $(\text{m}\cdot\text{s}^{-1})$ contributing to the lower tank level.

Since $S_d(f)$, in order to be bounded-variance, must be bounded and decreasing for $f > f_d$, $\sigma_{\max}(S(\text{j}f,\Gamma)S_d(f))$ turns out to be band-pass. By assuming that f_d and f_s have the same order of magnitude, we expect that $\max_f \sigma_{\max}(S(\text{j}f,\Gamma)S_d(f))$ occurs in the same frequency region. Fig. 7 (a) shows that, for $\underline{\gamma}=0.1$ (but the same expression applies to any $\underline{\gamma}$), the sensitivity low-frequency asymptote holds:

$$S_0(f,\underline{\gamma}) = \lim_{f\to 0}|S(\text{j}f,\underline{\gamma})| = (f/f_s(\underline{\gamma}))^3. \tag{75}$$

Therefore, if the decreasing profile of S_d for $f > f_d$ is approximated as follows (parameter values are in Table 2):

$$S_d(f) \approx \frac{S_{wd}}{2\pi f}\left(\frac{f_d}{f}\right)^2 (\text{m}\cdot(\sqrt{\text{Hz}})^{-1}), \quad f > f_d, \tag{76}$$

the bound $\tilde{\sigma}_{x,\max}(\underline{\gamma})$ on the tracking error RMS $\|\tilde{x}_k\|$, $k=1,2$ can be expressed by

$$\begin{aligned}\tilde{\sigma}_{x,\max}(\underline{\gamma}) &\cong \kappa\sqrt{\frac{p}{2\pi}}S_d(f_s)S_0(f_s,\underline{\gamma})\\ &\cong \kappa\frac{S_{wd}\sqrt{f_{SD}}}{2\pi}\frac{f_d^2}{f_s^3(\underline{\gamma})}\ (\text{m}),\end{aligned} \tag{77}$$

where $\kappa > 1$ is a conservative factor and $f_{SD} > f_s$ is an estimation of the spectral density bandwidth. Fig. 7 (b) compares the computed bound $\tilde{\sigma}_{x,\max}(\underline{\gamma})$ and the simu-

lated RMS $\|\tilde{x}_k\|$ versus the nominal $\underline{\gamma} \leqslant 0.49$. Since the computed RMS tracks the simulated RMS, it is employed to fix the bound $\tilde{x}_{\max}(\underline{\gamma}) = n\tilde{\sigma}_{x,\max}(\underline{\gamma})$, where $n = 3$, to the steady-state tracking error.

Table 2 Simulation parameters.

No	Parameter	Symbol	Unit	Value	Comment
1	Tank flow rate	β_k	mm/s	(5.0∼9.0)±20%	Equation (56)
2	Tank max level	$x_{k,\max}$	m	1.6∼1.7	Equation (56)
3	Pump max flow rate	$q_{\max}$	mm/s	18.5	Equation (56)
4	Pump rate quantum	$\rho_{qk}, k = 1,2$	mm/s	0.0045 (12 bit)	Equation (66)
5	Sensor noise	$\rho_{yk}(\sigma_{yk})$	mm	≅ 0.4 (0.4)	12 bit
6	Min sensor level	$y_{k,\min}$	mm	20	
7	Case 1: aperture	$\gamma_{1,2}$		0.1±5%	Equation (56)
8	Case 2: aperture	$\gamma_{1,2}$		0.45±5%	Equation (56)
9	Driving noise SD	S_{wd}	m/(s · $\sqrt{\text{Hz}}$)	0.015	Equation (77)
10	Cutoff frequency	f_d	mHz	0.88	Equation (77)
11	Upper tank pole	p	rad/s	0.021	Equation (77)
12	Simulation unit	T_s	s	1	
13	Switching times	t_{rj}	ks	0, 5, 20, 35, 50	$j = 0, \ldots, 4$
14	Tank 1 set points	$\underline{x}_{1j}$	m	0, 0.4, 0.8, 1.2, 0	$j = 0, \ldots, 4$
15	Tank 2 set points	$\underline{x}_{2j}$	m	0, 0.3, 0.9, 1.3, 0	$j = 0, \ldots, 4$

The bound $\tilde{\sigma}_{x,\max}(\underline{\gamma})$ applies to $\|\tilde{x}_k\|$, $k = 1,2$ for $t > t_r + \tau(\underline{\gamma}, |\Delta x_{krj}|)$, where the set point jump $|\Delta x_{krj}|$ occurs at time t_{rj} and $\tau_j(\underline{\gamma}, |\Delta x_{rkj}|)$ is defined by

$$\tau_j(\underline{\gamma}, \Delta x_{krj}) = \frac{\alpha}{2\pi f_s(\underline{\gamma})} \ln\left(\frac{|\Delta x_{krj}|}{\tilde{x}_{\max}(\underline{\gamma})}\right) \tag{78}$$

for $\alpha > 1$.

Fig. 7 (a), for $\underline{\gamma} = 0.1$, shows that the sensitivity low-frequency asymptote fits $S_0(f, \underline{\gamma})$ in (75). The degradation of $|S(\mathrm{j}f)|$ (overall closed-loop) with respect to $|S_m(\mathrm{j}f)|$ (state predictor only) due to a non-standard design is evident: the frequency BW reduction is of about three times, and, as soon as $\underline{\gamma}$ increases, it progressively degrades the accuracy as Fig. 7 (b) shows.

4.6 Simulated results

Simulation parameters are reported in Table 2. The nominal value of the uncertain parameters to be used in control design and implementation are reported together with their maximum uncertainty (in percent).

Control unit parameters and results are reported in Table 1. We distinguish between the SP sensitivity S_m and the overall sensitivity S. DT complementary eigenvalues $\gamma_k = 1 - \lambda_k$ are reported together with the relevant frequency BW.

The tracking error RMS in Table 1 has been computed by neglecting the transient profile between two successive set points and the zero set-point intervals. Fig. 11 shows the time history of the lower and the upper tank levels for $\underline{\gamma} = 0.1$ (Case 1). Whereas lower-tank levels accurately track their set points (true-level and set-point cannot be distinguished in Fig. 11 (a)), upper-tank levels fluctuate around their set points to allow compensation of random flows and of set-point switching transients. The level peaks indicate the latter compensation.

Fig. 12 (a), shows, for the Case 1, the pump commanded flows and the relevant set points. Pump flows are biased because of the parameter perturbations in Table 2, which confirms the efficient role of the random drift $\hat{x}_d$ of (68) in predicting and rejecting random flows and parameter perturbations. Pump flows saturate without significant oscillations, which confirms the CL eigenvalue design in equation (70).

Fig. 12 (b), compares the true tracking error $\tilde{x}_1 = x_1 - x_{1r}$ (solid line) and the measured tracking error $e_{1r} = \hat{x}_1 - x_{1r}$ (dashed line) of the tank 1. Due to a non-standard design, these errors are different only during the zero set-point intervals $t = [0, 5)$ ks and $t > 50$ ks. For $t > 50$ ks, except during the set-point switching interval, the true tracking error, though biased, is close to zero,

since $x_1 \to x_{1\mathrm{r}} = 0$. Instead $\hat{x}_1 - x_1 \to y_{1,\min} = 20\,\mathrm{mm}$, i.e., it equals the least sensor measurement (see Table 2, row 6). For $t < 5\,\mathrm{ks}$, both tracking errors should tend to fluctuate around zero since $x_1 \to y_{1,\min}$. However, since the upper tank levels saturate down to zero (see Fig. 11 (b)), they become incapable of compensating the lower-tank random flows. As a result, $\hat{x}_1 \to 0$, whereas x_1 diverges from zero.

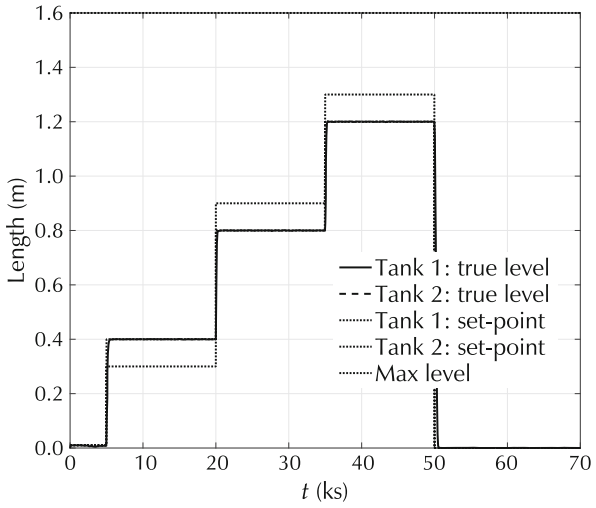

(a)

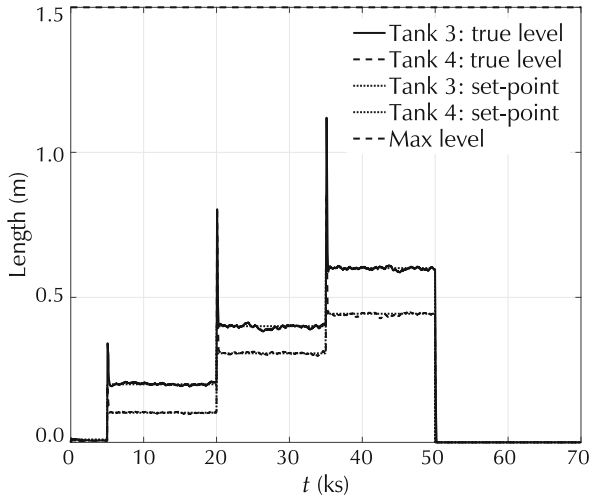

(b)

Fig. 11 Case 1. (a) Lower-tank levels. (b) Upper-tank levels.

Fig. 13 (b), shows the tracking errors of the Case 2. The same considerations as for the Case 1 apply, except that one of the upper-tank level remains close to zero for $t \in [5, 20)\,\mathrm{ks}$ (Fig. 13 (a)) and impedes the regulation of the tank 1 level. For $t > 20\,\mathrm{ks}$, the tracking errors increase as predicted by Fig. 7 (b), but, outside the transient intervals, they stay within the target bound.

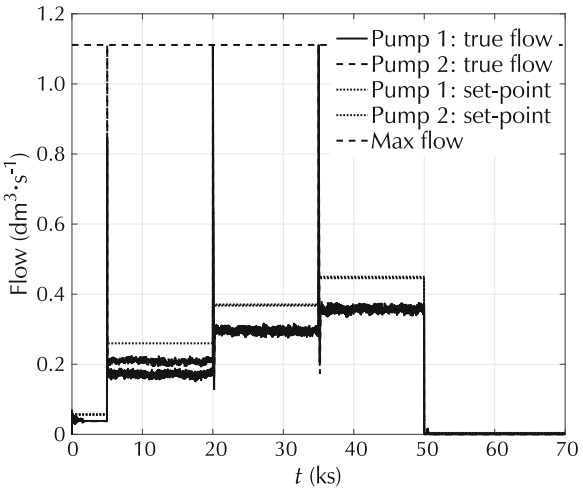

(a)

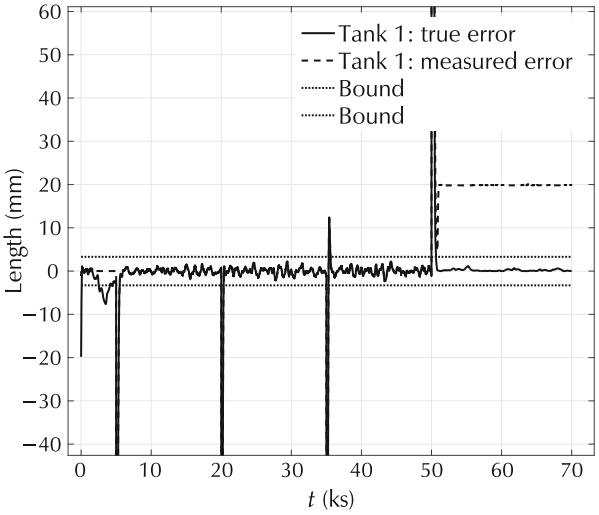

(b)

Fig. 12 Case 1. (a) Pump flow. (b) Tank 1 tracking errors.

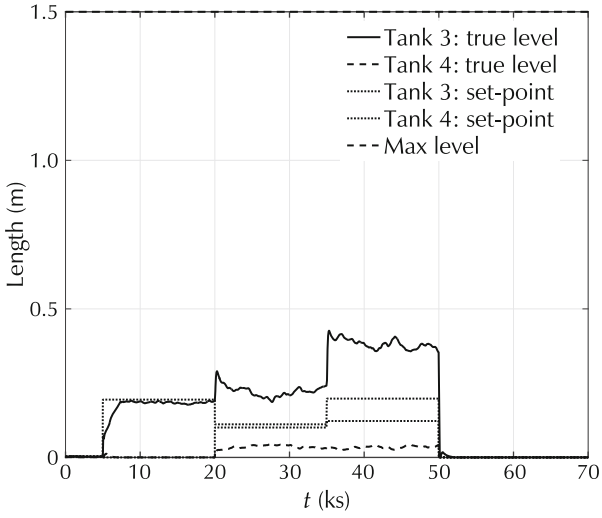

(a)

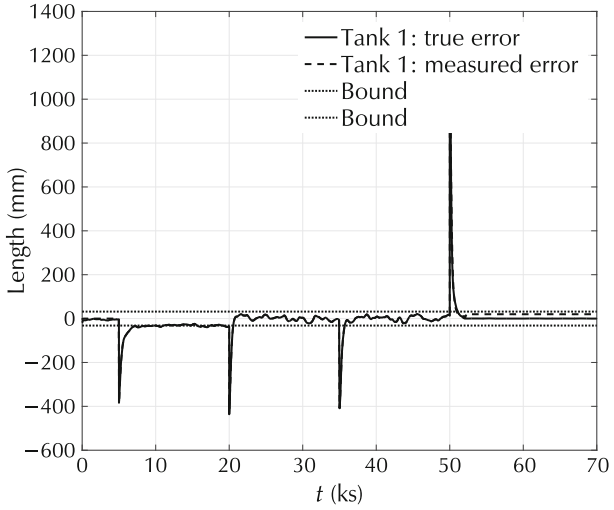

(b)

Fig. 13 Case 2. (a) Upper tank levels. (b) Tank 1 tracking errors.

As a conclusion, simulation results fit the accuracy requirements expressed by equation (77) and Fig. 7 (b).

5 Conclusions

The goal and effort of the paper was in the line of reconciling the modern control theory of [2] with the error-based design principle of the centenary PID of [5], still the work-horse of the closed-loop control systems in any application field. To this end, we have recalled in some detail the robust control theory of [10] with the aim of pointing out the concept and equations of the error loop, whose stability has been proved to be necessary and sufficient for the real plant stability. The forward path of the error loop is the cascade of the uncertain discrepancies between plant and model in series with the transfer functions of the modern control theory. The input signals of the error loop are reference signals and the bounded arbitrary (hence unpredictable) signals of the R. Kalman's theory (white noise process in the stochastic framework). The uncertain discrepancies are assumed to belong to parameterized sets, which, being bounded, imply that reality may generate incompatible outliers. The relevant detection and the consequent control system reconfiguration is outside of the paper scope. Error loop equations are converted by the embedded model control into design inequalities (similar to those of the H-infinity design methods), where control transfer functions are parameterized by the closed-loop eigenvalues to be designed (pole placement) versus stability/performance requirements and worst–case uncertainty. Frequency domain decomposition and transfer-function asymptotes allow the designer to find analytic inequalities capable of providing first-trial closed-loop poles and their margin versus stability and accuracy. The method is applied to a well-known multivariate control problem, which does not admit the feedback linearization normal form.

6 Acknowledgments

The authors are grateful to Prof. Z. Gao, Cleveland State University, Cleveland, Ohio, for his precious indications and suggestions.

References

[1] Z. Gao, Y. Huang, J. Han. An alternative paradigm for control system design. *Proceedings of the 40th IEEE Conference on Decision and Control*, Orlando: IEEE, 2001: 4578 – 4585.

[2] R. Kalman. On the general theory of control systems. *Proceedings of the 1st IFAC Congress Automatic Control*, Butterworths, 1960: 481 – 492.

[3] Z. Gao. Active disturbance rejection control: a paradigm shift in feedback control system design. *Proceedings of the American Control Conference*, Minneapolis: IEEE, 2006: 2399 – 2405.

[4] S. Bennet. The past of PID controllers. *IFAC Workshop on Digital Control: Past, Present and Future of PID Control*. J. Quevedo, T. Escobet (eds.). New York: Elsevier, 2000: 1 – 11.

[5] N. Minorsky. Directional stability of automatically steered bodies. *Journal of the American Society of Naval Engineers*, 1922, 34(2): 280 – 309.

[6] J. Han. From PID to active disturbance rejection control. *IEEE Transactions on Industrial Electronics*, 2009, 56(3): 900 – 906.

[7] E. Canuto. Embedded model control: outline of the theory. *ISA Transactions*, 2007, 46(1): 363 – 377.

[8] J. C. Doyle, G. Stein. Multivariable feedback design: concepts for a classical/modern synthesis. *IEEE Transactions on Automatic Control*, 1981, 26(1): 4 – 16.

[9] G. Zames. On the input-output stability of time-varying nonlinear feedback systems – Part I: Conditions derived using concepts of loop gain, conicity and positivity. *IEEE Transactions on Automatic Control*, 1966, 11(2): 228 – 238.

[10] F. Donati, M. Vallauri. Guaranteed control of almost-linear plants. *IEEE Transactions on Automatic Control*, 1984, 29(1): 34 – 41.

[11] E. Canuto, C. Novara, L. Massotti, et al. *Spacecraft Dynamics and Control: The Embedded Model Control Approach*. Oxford: Butterworth-Heinemann (Elsevier), 2018.

[12] M. Morari, E. Zafiriou. *Robust Process Control*. Englewood Cliffs: Prentice-Hall, 1989.

[13] K. H. Johansson. The quadruple-tank process: a multivariable laboratory process with an adjustable zero. *IEEE Transactions on Control Systems Technology*, 2000, 8(2): 456 – 465.

[14] J-J. E. Slotine, W. Li. *Applied Nonlinear Control*. Englewood Cliffs: Prentice-Hall, 1991.

[15] D. G. Luenberger. *Optimization by Vector Space Methods*. Hoboken: John Wiley & Sons, 1998.

[16] E. Canuto, W. Acuna-Bravo, C. Perez Montenegro. Robust control stability using the error loop. *International Journal of Mechatronics and Automation*, 2013, 3(2): 94 – 108.

[17] E. Canuto, C. Perez-Montenegro, L. Colangelo, et al. Active disturbance rejection control and embedded model control: a case study comparison. *Proceedings of the 33rd Chinese Control Conference*, Nanjing: IEEE, 2014: 3697 – 3702.

[18] E. Canuto, A. Molano-Jimenez, C. Perez Montenegro. Disturbance rejection in space applications: problems and solutions. *Acta Astronautica*, 2012, 72(1): 121 – 131.

[19] E. Canuto, A. Molano, L. Massotti. Drag-free control of the GOCE satellite: noise and observer design. *IEEE Transactions on Control Systems Technology*, 2010, 18(2): 501 – 509.

[20] E. Canuto, C. Perez- Montenegro, L. Colangelo, et al. Embedded model control: design separation under uncertainty. *Proceedings of the 33rd Chinese Control Conference*, Nanjing: IEEE, 2014: 3637 – 3643.

[21] J. Maciejowski. *Multivariable Feedback Design*. Wokingham: Addison-Wesley, 1989.

[22] C. Huang, E. Canuto, C. Novara. The four-tank control problem: comparison of two disturbance rejection control solutions. *ISA Transactions*, 2017, 71: 252 – 271.

[23] C. Huang, H. Sira-Ramirez. A flatness based active disturbance rejection controller for the four-tank benchmark problem. *Proceedings of the American Control Conference*, Chicago: IEEE, 2015: 4628 – 4633.

[24] P. P. Biswas, R. Srivastava, S. Ray, A. N. Samanta. Sliding mode control of quadruple tank process. *Mechatronics*, 2009, 19(4): 548 – 561.

Enrico CANUTO was born in Varallo (Piemonte), Italy. He received a degree in Electrical Engineering from Politecnico di Torino, Turin, Italy, where he joined the staff as Professor of Automatic Control in 1983, after ten years as a research staff of the National Electrical Metrology Institute G. Ferraris, Turin, Italy. From 1982 to 1997 he contributed to conception and implementation of the data reduction of the European astrometric mission Hipparcos. Technological studies in view of scientific and drag-free space missions, like Gaia and GOCE provided the opportunity of applying Embedded Model Control to drag-free control and to electro-optics. He contributed to the conception, design and implementation of the Nanobalance interferometric thrust-stand, capable of sub-micronewton accuracy. Recently he has been involved in the design of the orbit, formation and attitude control of the Next Generation Gravity Mission of the European Space Agency. He contributed to the Manufacturing Algebra. Currently he is cooperating with the Centre for Gravity Experiments of the Huazhong University of Science and Technology, Wuhan, China, in the field of space gravity missions. In the summer 2015 he was visiting researcher at the Northern China Electrical Power University, Beijing, China, applying Embedded Model Control to hydraulic case studies. His research interests cover all the entire field of control problems that are challenging because of complexity, uncertainty and precision. He is one of the authors of the book "Spacecraft Dynamics and control: the Embedded Model Control approach", Butterworth-Heinemann (Elsevier, 2018). E-mail: enrico.canuto@polito.it.

Carlo NOVARA received the Laurea degree in Physics from Universit?di Torino in 1996 and the Ph.D. degree in Computer and System Engineering from Politecnico di Torino in 2002. He held a visiting researcher position at University of California at Berkeley in 2001 and 2004. He is currently an Associate Professor at Politecnico di Torino, Italy. He is the author or co-author of more than 100 scientific publications in international journals and conferences. He has been involved in several national and international projects and in several research contracts in collaboration with Italian and European companies. He is the co-author of several patents in the automotive field. He is a member of the IEEE TC on System Identification and Adaptive Control, of the IFAC TC on Modelling, Identification and Signal Processing, and a founding member of the IEEE-CSS TC on Medical and Healthcare Systems. His research interests include nonlinear and LPV system identification, filtering/estimation, time series prediction, nonlinear control, data-driven methods, set membership methods, sparse methods, and automotive, aerospace, biomedical and sustainable energy applications. E-mail: carlo.novara@polito.it.

Luigi COLANGELO received a Bachelor's degree in Aerospace Engineering, in 2010, from Politecnico di Torino (Italy), and a Master's degree in Aerospace Engineering, in 2013, from Politecnico di Torino and Politecnico di Milano (Italy). In 2013, he joined the Department of Control and Computer Engineering from the Politecnico di Torino as a research assistant in the Space and Precision Automatics group. Then, in 2018, he received an ESA NPI-PhD in Control and Computer Engineering at Politecnico di Torino, in partnership with the European Space Agency and Thales Alenia Space, Turin, Italy. During his Ph.D. study, he worked on the modelling and control of spacecraft formation for the Next Generation Gravity Mission of the European Space Agency. In March 2018, he joined the Department of Electronics and Telecommunications, Politecnico di Torino, as a research affiliate. His main research areas include space guidance, navigation, and control, autonomous vehicles, and control theory. E-mail: luigi.colangelo@polito.it.